AN INVESTIGATION INTO SURFACE EFFECTS IN THIN FILM PLASTIC SCINTILLATORS

John P. Wentzel

1992

Submitted in fulfillment of the requirements for the degree of Master of Science in the Department of Physics at the University of Cape Town

ABSTRACT

An investigation into the luminescent response of thin film plastic scintillators as a function of their method of preparation is made. Investigations are carried out on NE102A and NE118 using four different methods of preparation. It is found that the Birks model for luminescence as a function of film thickness successfully explains the response in three of the four methods of preparation, but fails to explain the response of thin films prepared on a glass surface. These films show an unexpected non-linearity in their behaviour. It is proposed that the behaviour in these films can be explained in terms of the existence of surface regions in these films. A model based on the existence of these surface regions is prepared. It is further proposed that, in general, the luminescent response of thin films of plastic scintillator is dependant on their method of preparation.

CONTENTS

§1 INTRODUCTION

The development of thin film plastic scintillators (TFPS) can be traced back to 1970 when Muga et. al[1]. first described a new charged particle detector capable of registering the passage of very heavy ions with a low percentage energy loss. The detector consisted of a thin film of NE102A scintillator placed perpendicular to the face of a photomultiplier tube and coupled optically to the tube. It was found that the new detector had a good signal to noise ratio, fast pulse rise time, efficiency of detection of fission fragments of 100%, and was adequate for use in time-of-flight (TOF) measurements of heavy fragments. The first recipe for the step-by-step production of a TFPS was reported by Muga et. al[2], and consisted of evaporating a solution of plastic scintillator off a surface of water. The first study of TFPS response to transiting ions was reported by Muga et. al[3,4]. The TFPS response was found to be dependent predominantly on two factors, the velocity and atomic number of the transiting ion. Detailed investigations of the timing properties of TFPS was undertaken by Batsch and Moszynski[5]. A non-linear dependence of the scintillation efficiency of thin films of thickness below 3 μm was reported. The surface effect model of Birks[6] was used to explain the observed results. Batra and Schotter[7] later reported the response of NE102A TFPS's to ^{252}Cf fission fragments. A linear behaviour was reported for the residual energies of both the light and heavy fragments as a function of scintillator thickness traversed. The second major technique for the production of TFPS was reported by Ajitanand and Iyengar[8] and consisted of evaporating a solution of plastic scintillator off a glass surface under vacuum. Brooks et.al[9] investigated the response of NE102A TFPS to fragment ions from ^{252}Cf. They reported a non-linear response as a function of TFPS thickness. An attempt was made to explain the result in terms of the surface effect model proposed by Birks. McLeod[10] later confirmed the findings of Brooks.

The results on the response of TFPS to fission fragments, as a function of the film thickness, is contradictory. While the findings of Brooks, and McLeod indicate a non-linear TFPS response as a function of film thickness, those of Batra and Schotter indicate a linear TFPS response as a function of film thickness. The method of preparation of the films differed. Batra and Schotter used the method of Muga, while Brooks and McLeod used the method of Ajitanand. The published results are all for NE102A scintillator. The present study aims to undertake a detailed investigation of the luminescence of thin film plastic scintillators as a function of their thickness. Four different methods of TFPS preparation were used to determine whether the response of the film is dependent on the method of preparation. The four methods employed, and which will be described in detail later, are (i) the method of Muga, referred to as water based films (WBF), (ii) pressed films using a specially designed press, referred to as pressed films (PF), (iii) films prepared using the method of Ajitanand and Iyengar, referred to as non-annealed glass based films (non-annealed GBF) and, (iv) films prepared using the method of Iyengar and then annealed (annealed-GBF). Two types of plastic scintillator NE102A and NE118, which are structurally different, were used in the measurements to determine whether the material structure affects the film response. A range of film thicknesses from 2 to 10 μm was chosen to perform the measurements on. This ensured that for all the film thicknesses the fragments passed through the film.

§2 SCINTILLATORS

It would be beyond the scope of this chapter to discuss the general physics of luminescence of scintillators. This may be found in more specialised monographs (Pringsheim[11], Birks[6]). The origin and principle features of luminescence and scintillations in organic systems will be described in this chapter.

§2.1 STRUCTURE

A scintillator may be defined as any material which will emit a brief pulse of light, or scintillation, when it interacts with a high energy particle or photon. Luminescence, the emission of light (visible or ultraviolet) with a characteristic spectrum, following the absorbtion of radiation normally of higher energy than the emission, is a property associated with conjugated and aromatic organic molecules. These aromatic organic molecules (benzoid ring molecules) have a cloud of delocalised π-electrons associated with it, and it is the excited states of these π-electron systems which are responsible for the luminescence seen in scintillator molecules. Plastic scintillators are aromatic compounds with planar molecules built up mainly from condensed or linked benzoid rings (King[12]). Practical scintillators can be formed by combining suitable organic compounds. Scintillators can be classified as unitary, binary and ternary, or higher, according to the number of compounds they contain (Brooks[13]). Scintillators also come in three types: crystal,liquid and plastic. Crystal scintillators are usually unitary compounds that occur naturally, such as anthracene. Liquid scintillators are prepared by combining combinations of compounds in the presence of a suitable solvent. Plastic scintillators are prepared in much the same way as liquid scintillators, but the solvent and solute compounds that make up the scintillator are mixed in the presence of a polymerising agent. The starting material and the conditions under which the resultant polymer is formed determine the scintillation properties of the resultant plastic. The plastic scintillator, NE102A, consists of 10 g/l of p-terphenyl (solute) in polyvinyltoluene (solvent). NE118 plastic scintillator consists of the same materials, but a cross-linking polymer agent is added, resulting in a scintillator that has a different structure and different properties to that of NE102A.

§2.2 SCINTILLATION PROCESS

The scintillation process in organic plastic scintillators can be divided into two parts, primary and secondary. Primary processes correspond to transfer of energy from the ionising radiation to the bulk constituent. The concentration of the secondary and other constituents are normally sufficiently small so that their direct excitation can be ignored (Brooks[13]). The primary excitation includes molecules ionised or excited by direct coulomb interaction up to several molecular diameters from the particle path. In addition, secondary electrons released in close encounter with the particle cause further excitations as they are brought to rest in the material. The secondary processes are those which compete for the excitation energy of the bulk material. The scintillation emission is associated with the decay of π-electronic states excited by the incident particle, by secondary electrons produced by the particle, by ion recombination, or by X-ray or ultra-violet photons emitted following ion

recombination (Brooks[13]). At ordinary temperatures, the molecule will normally occupy the ground state. Depending on the amount of excitation energy absorbed, various higher energy states and their associated vibrational states will be occupied. Vibrational energy will generally be rapidly dissipated as heat by collisions with surrounding molecules or excitation of lattice vibrations. After this process the molecule will possess only electronic excitation energy which may also be converted into vibrational energy. Alternately, the excited molecule may emit fluorescence by transition to the ground state from any of the higher excited states. From studies on the spectra of scintillators, it has been found that fluorescent emission from the higher states is non-existent, and that the only emission occurs from the first excited state (Brooks[14]). Excited states higher than the first undergo rapid internal quenching to the first excited state and then a slower fluorescent decay to the ground state. Studies by Koski[15] on plastic-fluor binary scintillators indicated that, in an efficient binary system, the incident ionising particle deposited energy almost entirely in the bulk solvent, but that the final scintillation emission originated almost entirely from the solute, showing that an efficient transfer of excitation energy occurs from solvent to solute. Direct evidence of energy transfer in organic crystals, and scintillating solutions were reported by Ageno and Cortelessa[16], and Ageno and Querzoli[17]

§2.3 ENERGY TRANSFER

By radiative and non-radiative mechanisms, the excitation energy deposited in the scintillator moves rapidly from initially excited atoms or molecules to others. Because of this transfer, each luminescence process generally involves several molecules rather than just a single molecule. Work by Birks and Kuchela[18] indicated that for plastic scintillators, radiative transfer can be neglected, and that the energy transfer is almost entirely non-radiative. If there is sufficient energetic coupling between two molecules transfer of excitation energy from one to the other may occur. This process requires some amount of mutual coupling between the electronic systems of both molecules, and can therefore take place only over limited distances. The π-electrons of a scintillator molecule are not stationary in their clouds but correspond to rapidly alternating electric waves. This results in rapidly varying dipoles in the electrical structure of the molecule (although its time averaged dipole moment may be zero) and these can induce in neighbouring molecules other dipoles in phase, and in interaction with themselves. Forster[19] has developed a mechanism to explain this kind of dipole-dipole transfer process. The probability of such a transfer of energy is proportional to the Forster overlap integral, J, defined by

$$J = \int_0^\infty f_o(\nu)\epsilon_1(\nu)\left(\frac{d\nu}{\nu^4}\right)$$

where $f_o(\nu)$ is the quantum emission spectrum of the solvent, and $\epsilon_1(\nu)$ is the absorbtion spectrum of the solute, ν being the frequency of the radiation.The probability of energy transfer is also proportional to the inverse sixth power of the distance, R, between the two molecules. Surrounding each molecule is a sphere, radius R_o, defined by the condition that the probability of energy transfer $\geq$ competing processes. The results of several experimental studies indicate that the

Forster theory is applicable to solvent-solute transfer in plastic scintillators. Swank and Buck[20] found that the non-radiative solvent-solute transfer in plastic scintillators occurs by the Forster process, and that the efficiency of the process depends on the nature of the solute and the magnitude of the critical radius, R. The most direct test of the applicability of the Forster theory to plastic scintillators was done by Basile[21], who obtained excellent agreement with the Forster relation.

§2.4 QUENCHING

Quenching is the loss of energy that would normally be available for luminescence to processes that do not result in further transfer of energy. They are responsible for the non-linear response of luminescence, L, as a function of energy, that is observed (Birks[6]). The two most important types of quenching that occur in plastics are ionisation quenching and the surface effect. Black[22] proposed that if the specific energy loss of the incident particle was very high, quenching due to double excitation may take place in the primary column, and that the observed fluorescence would then be mainly due to the fluorescent emission of the secondary region. Measurements by Meyer and Murray[23] on alkali halide crystals indicate that as the specific energy loss in the primary column increases, the differential luminescence of the primary column decreases. This kind of quenching is referred to as ionisation quenching. For heavily ionising particles such as fission fragments incident on plastic, ionisation quenching will lead to a saturation or decrease of the luminescent response as the differential energy loss increases. These predictions are consistent with the observations of Jentschke et al[24]. The surface effect was first proposed by Birks to explain the observed response of organic crystals to short range particles. When the range of the particle was very small, or the thickness of the crystals reduced below a certain thickness, the efficiency of the scintillator dropped to half the expected value. Similar effects were observed by Wright in anthracene. Birks[25] proposed that for short range particles the energy escaped from the surface of the scintillator before it was converted into luminescence. An expression was devised to relate the drop in the efficiency Φ near the surface to the mean free path for non-radiative transfer in the scintillator where

$$\phi = 1 - \frac{1}{4}\left(\frac{r}{a_o+2}\right)\exp\left(-\frac{r}{a_o}\right)$$

In the expression above, r is the distance variable and a_0 the mean free path for non-radiative transfer. Below the critical distance a_0 the efficiency rapidly drops to half the expected value. Birks[26] modified the equation in a subsequent paper, but calculated that the mean free path for non-radiative transfer in plastics was 3-7 μm. For scintillators with mean thicknesses below that of the mean free path for radiative transfer, the luminescent response will be less than that expected on the basis of results for thicker films. Escape of the excitation energy is not the only form of surface quenching that may occur. The surface of anthracene, and to a lesser extent that of other organic crystals and plastic scintillators, deteriorates on exposure to the atmosphere, probably due to oxidation (Wright[27,28]). Another possible cause of reduced surface scintillation efficiency is back scattering of the primary electrons out of the scintillator (Taylor et.al.[29]). There are several other forms of quenching that

have considerably less impact than those discussed above, and which have been left out of the discussion. Full details of these other forms of quenching can be found in Schram[30].

§2.5 LUMINESCENCE

The response, L, of organic scintillators is a non-linear function of the particle energy, E (Birks[6]). One of the most widely-used expressions relating the specific luminescence to the specific energy loss of the particle, is the semi-empirical relation due to Birks[31]. Birks' proposed a relation between the specific fluorescence, dL/dx, representing the scintillation photons produced per unit distance, and dE/dx.

$$\frac{dL}{dx} = \frac{A\frac{dE}{dx}}{1 + kB\frac{dE}{dx}} \qquad 1$$

where BdE/dx represents the density of quenching centres produced per unit distance by the incident particle, and the specific fluorescence is reduced by a factor (1+kBdE/dx) due to quenching processes characterised by a quenching parameter, k. A modified relation including quenching effects of the second order in dE/dx was proposed by Chou[32]. The second order effects were first proposed by Furst and Kallman[33], and these included processes such as double excitation,interaction of excited molecules, and triplet-triplet interaction. Chou's expression has the form

$$\frac{dL}{dx} = \frac{A\frac{dE}{dx}}{1 + B\frac{dE}{dx} + C(\frac{dE}{dx})^2} \qquad 2$$

where the constant C can be positive or negative. A different treatment by Wright[34] concluded that bimolecular, or double excitation processes are extremely rapid compared to the energy migration out of the primary column, and can be neglected when considering primary quenching. This leads to a third relation for the differential luminescence response

$$\frac{dL}{dx} = (\frac{A}{2B})\ln(1 + 2B\frac{dE}{dx}) \qquad 3$$

The similar behaviour of the three equations in the limit of small dE/dx can be demonstrated by putting $C=\frac{1}{2}B^2$, and expanding in powers of BdE/dx, which gives the same expression to second order for the three relations. The three relations predict a linear response

$$L(E) = \acute{A}E + L_o \qquad 4$$

within this limit. In the limit of high dE/dx, the three relations predict different behaviours. Following Wright, the specific luminescence should increase continuously with dE/dx, and according to Birks should tend to a constant saturation value. Depending on the sign of the constant, C, in Chou's work, he predicts that the

specific luminescence may go through a maximum and decrease thereafter. Voltz et al[35] have formulated a theory of the scintillation response that takes account of the spatial distribution of primary excitations, and of the kinetics of the prompt and delayed scintillation components. This work also predicts that dL/dx will go through a maximum. The term used is an analytic one, and is far more complicated than the other relations reviewed. A review of the response of alpha's, electrons and protons by Brooks[14] indicates that the relation of Birks is more accurate in describing the data for the more heavily ionising alpha's than that of Wright. Works by Newman[36], Muga and Griffith[37] indicate that the response of heavily ionising particles follows the relations of Birks and Chou, and should describe the luminescent behaviour of fission fragments quite accurately.

§3 POLYMERS

This chapter is not meant to give a full account of polymers; only those aspects of polymers that could possibly be important in explaining the behaviour of thin film plastic scintillators are described.

§3.1 POLYMER MORPHOLOGY AND STRUCTURE

Polymers are long chain molecules containing thousands of individual atoms or groups of atoms. The chain usually consists of one or more kinds of atom or molecule that is repeated many times. In polymers, all primary chemical bonds are covalent bonds. These bonds are strong, stable, and the polymer molecules built from them can generally be broken down or modified only by the action of vigorous thermal or chemical forces. The electrons of the covalent bond are not shared equally by both the participating atoms, and the bond has a non-zero dipole moment. In a polymeric substance, if some of the individual polymer chains show a mutual alignment this region of the polymer is termed a crystallite. Polymers are classified in terms of this[46]. An amorphous polymer is one with no crystallites. The chains in the polymer are randomly orientated with respect to each other. An unorientated crystalline polymer is one which has considerable crystallites, but the crystallites are essentially randomly orientated with respect to each other. An oriented crystalline polymer is one in which some of the polymer chains are aligned with respect to each another. Elastomers are intermediate in character between amorphous and crystalline polymers, and posses elastic behaviour. Both NE102A and NE118 are examples of amorphous polymers. Polymer chains also differ, although their basic bond structure is the same. The two kinds of chains of interest are linear and cross-linked chains. A linear chain is one that essentially lies in a straight line. The forces which operate between the chains linking them in non-primary bonds are weak electrostatically based van der Waal's forces. NE102A is a linear polymer. Cross-linked polymers have the individual chains linked to each other by covalent bonds at various points along the polymer chain. There are thus strong covalent links as well as weaker van der Waal's links, joining the individual chains. Such a polymer can be viewed as a 3-dimensional network. The degree of cross-linking in such a polymer is related to the number of covalent bonds linking the individual chains. The presence of cross-linking, and the degree of cross-linking, affects the physical properties of the polymer. NE118 is a cross-linked polymer. Figure 1 shows a schematic drawing of the structure of NE102A and NE118.

§3.2 POLYMERS IN SOLUTION

Linear (NE102A) polymers behave differently to cross-linked or network polymers (NE118) in solution. For linear polymers the solvent molecules break the weak V.D. Waals forces between the individual chains and the polymer undergoes complete dissociation. The end-to-end separation, r, of the polymer chains, will be continually changing in solution, and since there are many chains of different lengths, a root mean square (RMS) length is used to characterise the polymer chains in solution.

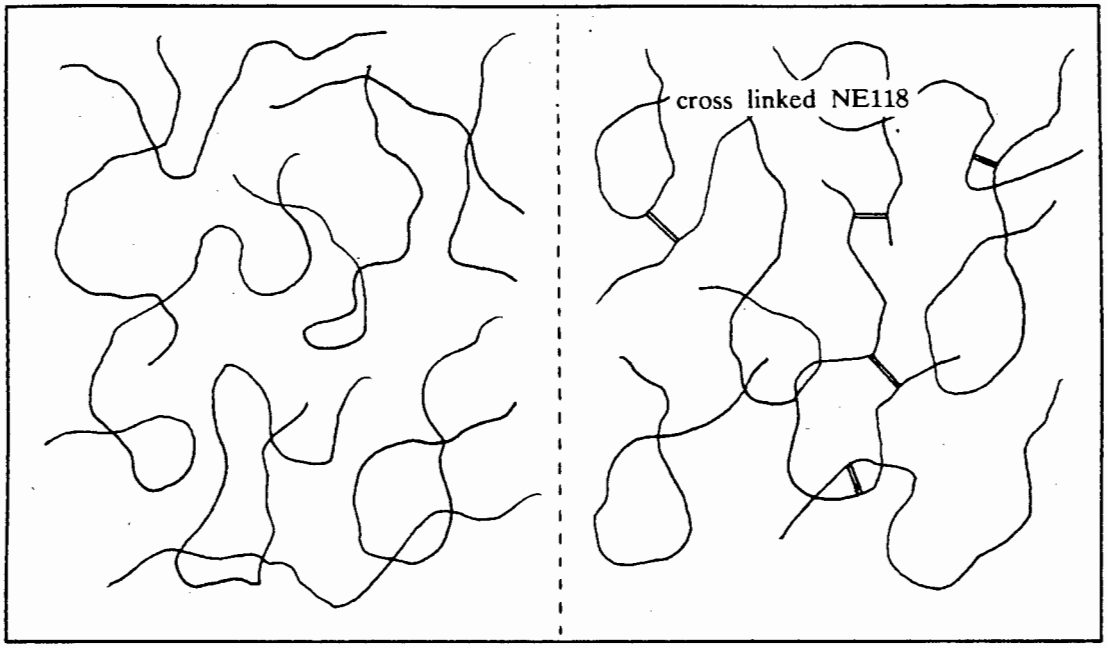

Figure 1. Schematic diagram of the structure of NE102A and cross linked NE118 plastic scintillator, respectively.

If there are N_i polymer molecules in solution each with length r_i then

$$\langle \overline{r^2} \rangle^{\frac{1}{2}} = \left(\frac{N_1 r_1^2 + N_2 r_2^2 + \ldots + N_i r_i^2}{N_1 + N_2 + \ldots + N_i}\right) \qquad 5$$

it can further be shown[47] that

$$\langle \overline{r^2} \rangle^{\frac{1}{2}} = n^{\frac{1}{2}} l \qquad 6$$

where l is the individual monomer length, and n the average number of monomers in the polymer molecule chain. When in solution, the polymer molecules dissociate completely from each other, and behave like individual molecules. The spatial distribution that the polymer molecule occupies is not strictly defined, but each molecule can be viewed[48] as being distributed within a sphere of radius r. Kuhn[49] notes that when the chain length is great, the solvent within the region occupied by the randomly coiled molecule moves with the molecule as a unit. Thus the molecule behaves in much the same way that a rigid sphere would. A linear polymer chain may undergo a dramatic coiling in solution. As an example, a linear polymer chain containing 10 000 structural units each of length 2 A will have a linear chain length of 20 000 A, but may have r = 200 A only. Figure 2 shows a schematic drawing of NE102A molecules in solution.

Cross-linked polymers behave in a different way to linear polymers in solution. A three-dimensional network polymer is incapable of dispersing completely[50]. In the presence of a solvent, the network polymer absorbs the solvent leading to the swelling of the network. As the network is swollen the chains between the network junctions are required to assume elongated configurations. An elastic retractive force in opposition to the swelling develops, and a state of equilibrium swelling is reached in which these two forces are in balance. With low degrees of cross-linking, the

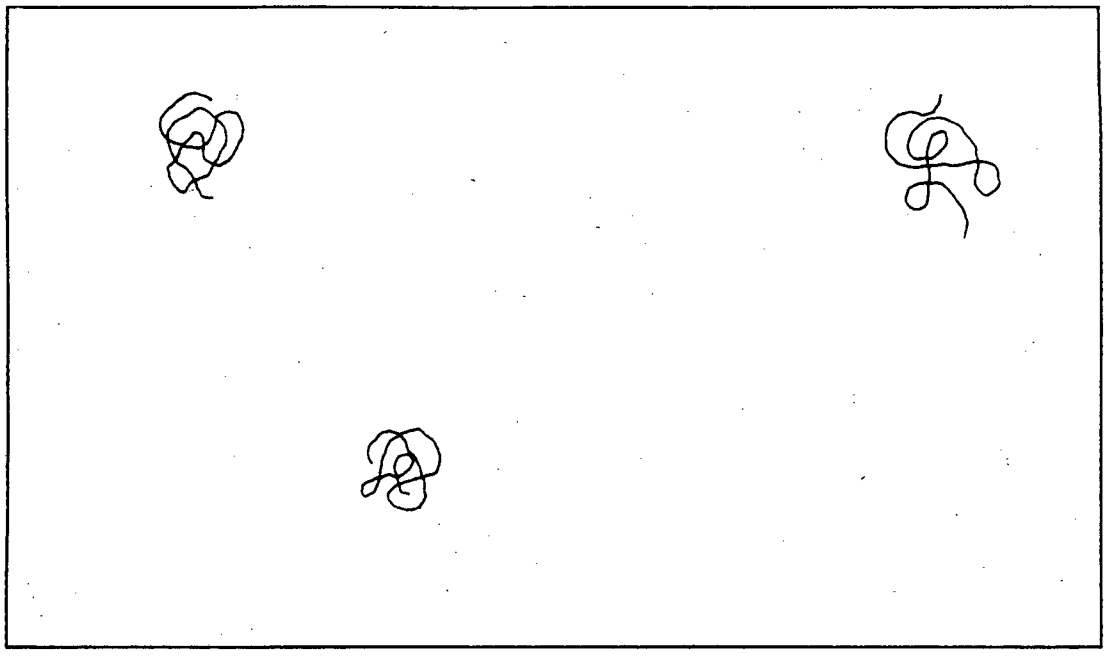

Figure 2. Schematic diagram of NE102A in solution.

resultant structure with solvent may contain no more than 2% polymer by volume. Although not strictly dissolving, the structure will for all practical purposes still behave like a solution. Figure 3 shows a schematic diagram of the NE118 scintillator in solution.

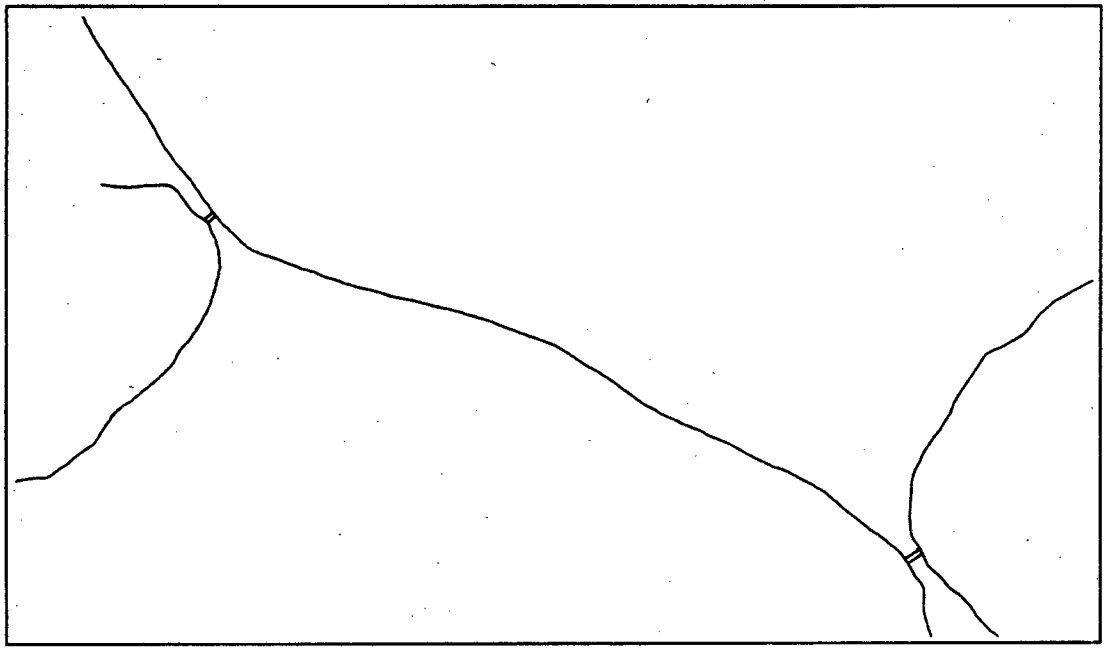

Figure 3. Schematic diagram of NE118 polymer in solution.

§3.3 POLYMER CRYSTALLIZATION UNDER STRESS

When polymers solidify in the presence of an applied stress, the resultant structure is different from that of an unstressed polymer. Keller and Machin[51] studied thin films of polyethylene crystallized under stress. In all cases they observed crystals that grew along axes that lay in a direction perpendicular to the stress direction. This

behaviour was also observed when a cross-linking agent was added to the polyethylene. Palin[52] reported that if the crystallization occurs in the absence of external forces and the orientation of the chains are random, then if such a material is cooled past its melting point under the influence of an external stress, the direction of the crystallites will be orientated. He noted that the effect also occurs for amorphous polymers. Hall[53] noted that for crystalline polymers, crystallisation from melts under stress gives rise to a fibrillar rather than a spherulitic morphology. In these cases the crystalline fibrils develop along a direction normal to the applied stress. In general, for polymers crystallized under stress, the molecular chains align themselves in a direction perpendicular to the direction of the applied stress.

§3.4 POLYMER SURFACE MORPHOLOGY

The existence of an interface can change the morphology of polymer molecules lying in its vicinity. Eby[54] reported that cooling the surface of a polymer melt in the presence of an interface leads to the formation of a surface region in the polymer. Eby measured the diffusion of ethane in polyethylene, and found that the diffusion rate was greatest in the sample with the thickest surface layer. The results pointed to the existence of surface layers with different structural and physical properties to that of the bulk material. Kwei et. al[55]. found that the structure which grows in these surface regions can propagate only in one principal direction, normal to the surface since the growth in lateral directions is restricted by neighbouring spherulites. These conditions lead to the formation of surface regions in which only very narrow divergent sectors develop and give an overall rod like appearance. In their experiment they measured the Young's modulus of moulded sheets of polyethylene and polypropylene. Some of their results are shown in fig 4.

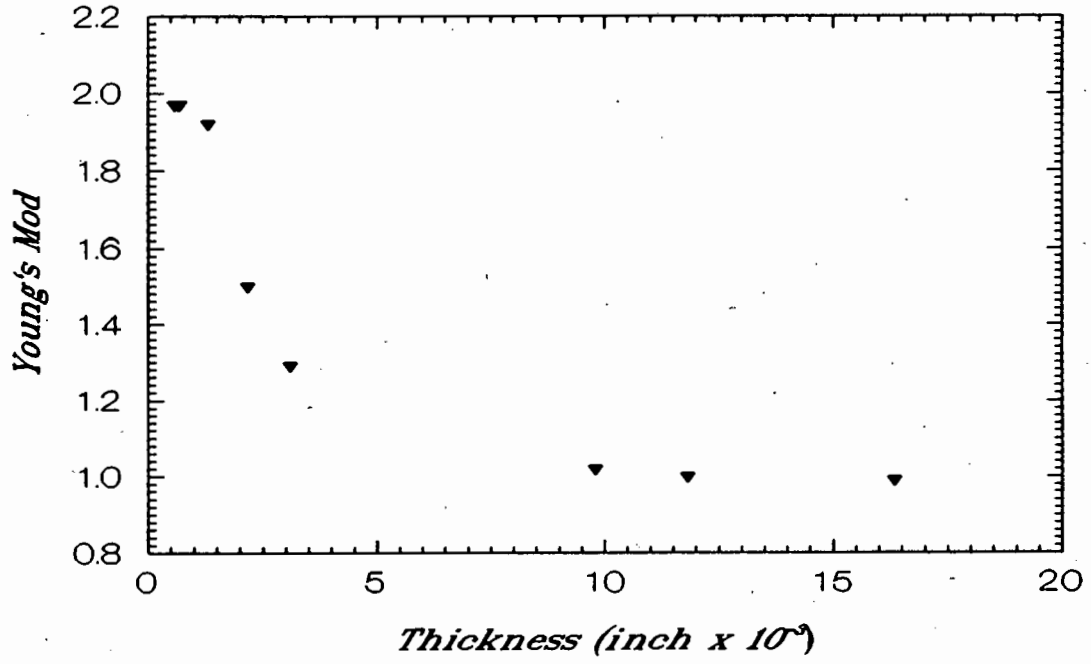

Figure 4. Young's modulus for polyethylene as a function of sample thickness. (Kwei[55])

They explained their results in terms of surface regions. For the very thick regions the properties are dominated by the bulk of the sample, and for the very thin samples, the properties were that of the surface region. They postulated that at some

thickness the sample became all surface region. In between these two regions the properties are determined by the ratio

$$\frac{t_s}{t - t_s} \qquad 7$$

where t is the total thickness, and t_s is the thickness of the surface region. Fritsch et. al[56]. noted that the surface regions originated due to the anisotropy of the intermolecular force and also because for the thin films, longer-ranged cooperative phenomenon can come into play. They also note that the transcrystalline surface regions have different mechanical properties, diffusion and solubility coefficients, and surface properties, from the bulk interior of the polymer.

§4 EXPERIMENTAL SETUP

Sections 1 to 3 have given a theoretical introduction to polymers and scintillators. The remaining sections describe the experiments, including data analysis and conclusions. The following chapter describes the methods of preparation of the 4 kinds of thin film; the water based, pressed, annealed glass based and non-annealed glass based, as well as the procedures for testing uniformity and measuring film thickness. It also contains the electronic setup and description of the analysis that was performed on the recorded data

§4.1 WATER BASED FILMS

The method for the preparation of the water based films followed that of Muga[2]. For the NE102A films, three solutions of NE102A in xylene were prepared. Chips of solid NE102A were dissolved in scintillation grade xylene to produce solutions of strength 6.26 mg/ml, 10.51 mg/ml and 21.00 mg/ml. The mixtures were left to stand undisturbed for 24 hours to ensure complete dissolution of the NE102A. To ensure that no impurities had entered the mixtures, or that any errors had entered in the preparation, two separate containers of each solution were prepared from separate chips of scintillator. A circular porcelain dish of diameter 8cm and depth 5cm was half filled with water. A 5ml pipette was used to deposit a quantity of the solution on the surface of the water. An upturned 4l glass beaker was placed over the porcelain dish to eliminate any air current's. The dish was then left to stand for 12 to 20 hours. As the xylene evaporated, the solid film was left floating on the surface of the water.

The long standing time was necessary because of the slow rate of evaporation of the xylene. A cardboard disc of thickness 0.25 mm and diameter 40mm was slipped under the floating film and the film then lifted out of the water. The disc with the film on top was placed upside down on a layer of absorbent paper on a wooden surface. The cardboard disc was slid to one side of the film and removed. Any creases in the wet film were very carefully smoothed out with a pair of tweezers and a second layer of absorbent paper was placed on the film. A lead block of mass 4.5 kg was then placed on top of the film and it was left to dry for about 30 minutes. The dried film was strong enough to be handled with the bare hand. It was found that by holding the pipette at varying heights above the surface of the water, and carefully depositing the solution on the surface it was possible to control the size of the circle that the solution formed when it was spread out on the surface. By using this technique and by varying the quantities and the strengths of the solutions, it was possible to produce a range of thicknesses. The method, although producing excellent films, suffers from several drawbacks. The method is very time consuming, taking many hours to produce one film. The method is unable to produce a thickness "on demand", i.e. if one wanted a film of say 5 μm, several films had to be produced in the hope that one of them would be close to the desired thickness. Uniformity was tested for each film. The very thin films (1.5 to 4 μm) produced by this method are very difficult to handle when wet, consequently it was not possible to produce a successful film thinner than 2 μm. For testing of the film uniformity, and measurement of the film thickness, the film was glued to a circular cardboard ring of diameter 5cm and inner diameter 4.28 cm. A variation of the Michaelson

interferometer was used to measure the thickness and check the uniformity. The set-up used was similar to that of McLeod[10], and utilised a monochromatic sodium light, and a white light source in a split field of view arrangement. The Michaelson interferometer was calibrated using the wavelength of the ^{22}Na yellow doublet. The uniformity of the films was easily determined using this technique. After the film thickness was measured the film was cut from the cardboard disc and mounted for the data collection

Several other techniques were tried to produce the films in a more efficient way. In one of the methods the same porcelain dish was half filled with water and placed on a heating pad. The water was heated to a temperature of 60°C and maintained at that temperature. A small amount of solution was placed on the surface of the water and an inverted 4l glass beaker placed over the dish. Although this technique held out the promise of faster preparation times relative to the chosen method, minute bubbles of air formed in the water on the bottom of the porcelain dish, at that temperature. As they rose to the surface, they produced small bubbles in the surface of the film, leading to non-uniform films that had small holes in them. The second of the methods tried was that of Batra and Schotter[3]. A rubber O-ring of mass 25 g and inner diameter 5 cm was floated on the surface of the water. A quantity of solution sufficient to cover the inner area of the O-ring was deposited in it. The advantages of this method, as found by Batra and Schotter, were increased film uniformity, as well as a known area over which the solution would spread, allowing one to use the solution volume and concentration to gain an estimate of the resultant thickness. The major problem encountered in this method was the difficulty in removing the completed film from the O-ring. Piercing the film near the inner edge on the O-ring often resulted in tearing, and most of the completed films were destroyed in trying to remove them from the O-ring. Greasing the O-ring, using different O-rings or using a metal ring slid under the complete film to try to lift it from the O-ring, failed to produce success rates sufficient to render the technique practical.

§4.2 NON-ANNEALED GLASS BASED FILMS

The glass based films were prepared using a method similar to that of Ajitanand and Iyengar[8]. Several glass discs of mean diameter 36.2mm and thickness 0.30mm were used in the preparation of the glass based films. The glass discs were carefully cleaned with scintillation grade xylene and placed on a brass mounting inside a vacuum chamber. The mounting had been carefully levelled using a small spirit level. After depositing the required volume of solution on the glass, the chamber was slowly evacuated to a pressure of about 10^{-4} Torr. The film was then left for about 30 minutes to dry out completely. Once dried, the film was ready for mounting in the detector. Though we used the film on the glass, it is possible to remove the film from the glass by leaving the glass disc in a beaker of water. The film will then float off. Wiping the glass disc using a tissue dampened with teepol before any solution is deposited, aids in its subsequent removal by floatation. From the diameter of the glass discs and the known density of the two plastic scintillators, depositing a known volume of solution on the glass results in a film with thickness given by

$$t = \frac{4CV}{\rho \pi d^2} \qquad 8$$

where d is the diameter of the glass disc, C the concentration of the solution, V the volume of solution deposited on the glass disc and ρ the density of the scintillator. The thickness and the uniformity of the film was checked using the Michaelson interferometer. Because we needed to use the glass based films in more than one way (§4.3) we could not remove the films from the glass base. Several films were removed and checked using a Michaelson interferometer for thickness and compared with the predictions of equation 10. The results of these measurements were used to complete a calibration curve of the glass based films. The calibration curve is shown in fig 5. Extrapolation of the fitted curve to zero indicates that equation 8 fails to provide accurate predictions of thicknesses less than 1.5 μm.

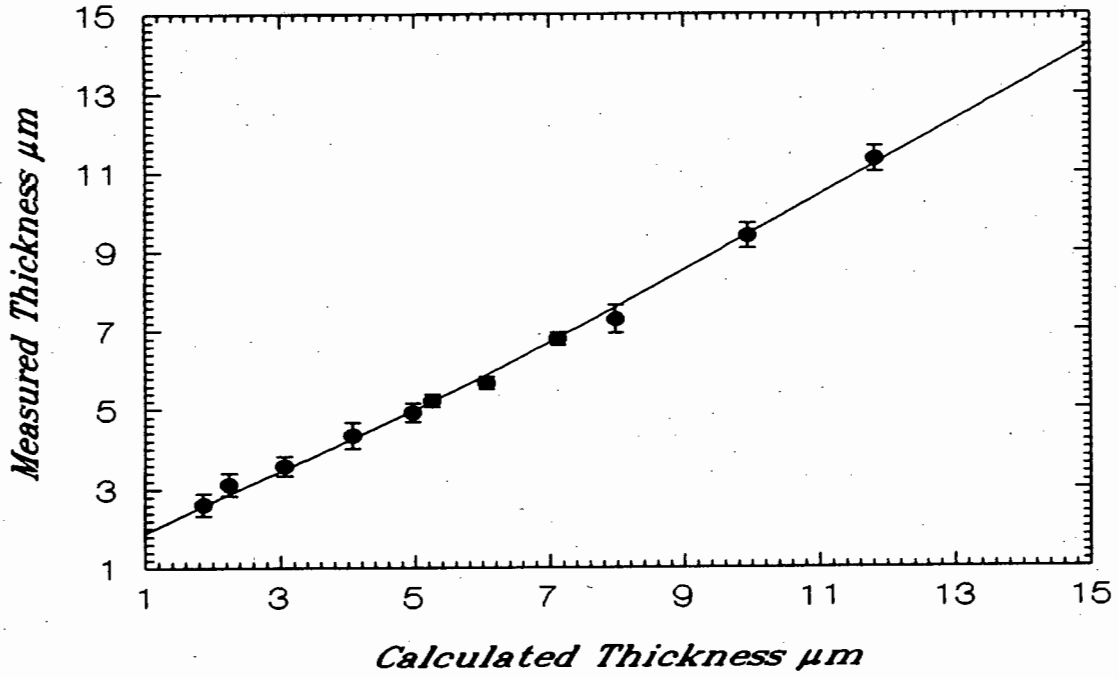

Figure 5. Glass based film calibration curve

The equation for the fitted line is

$$T_m = \exp(-T_c^2 a) + bT_c \qquad 9$$

where T_m is the measured thickness and T_c is the calculated thickness using equation 11. The values of the two fitted parameters are

$$a = 0.055 \pm 0.009$$
$$b = 0.949 \pm 0.006$$

This method of preparation was probably the best of the four methods tried. The films produced have excellent clarity and uniformity. The films are produced in minutes rather than hours, and the film thickness can be predicted beforehand and checked afterwards.

§4.3 PRESSED FILMS

The method of preparation of the pressed films follows that of Largiss[57], but differs in that the thicknesses produced are much smaller than those in his work. A specially designed and constructed rig was produced for the annealing and the pressing of thin films. The rig consists of two flat discs of thickness 6cm and diameter 8cm, the one above the other. The bottom disc is fixed and the upper one, held in place by four strong steel pillars, is held up by a spring. A hydraulic piston pushes the upper disc down against the spring and a pressure of up to 9000psi can be applied to the top disc, allowing a force of up to 6200 N/cm^2 to be applied to any substance placed between the two discs. Special care has been taken in the design to keep the two discs parallel during the application of pressure. Each disc contains a heating element connected to a variac by means of which the heating current and hence the temperature can be controlled. The temperature is read off a digital thermometer. Photographs of the press are presented on the following page. The preparation of the NE102A films proceeded as follows. The press was heated to 105°C and maintained at that temperature throughout the process. A small chip of solid NE102A was placed at the centre of the lower disc and the gap between the two faces reduced to about 1mm. The solid scintillator was allowed to melt and the faces were brought together. Initially a pressure of 1500 psi was applied for 1 minute before being released for 20 seconds. Pressure of 2500 psi was then applied for 2 minutes before releasing. Finally pressures of 3000 psi and above were applied and the current to the heating elements terminated, allowing the film to cool. This cooling took about 20 minutes. Once the temperature had fallen to about 30°C the pressure was released. The film was removed using a thin blade. The procedure of applying and releasing pressure successively was necessary to allow the melted scintillator to spread. Although the method produced films in a relatively straightforward manner, several difficulties with the method were encountered. The biggest problem was that as the film spreads out, the pressure on it decreases because its area increases. For the same applied force, the pressure is much higher initially (smaller area) than later. This, coupled with the viscosity of the film, meant that resistance to further spreading increased and a point was reached where increasing force did not result in any significant further spread of the melted scintillator. This is particularly a problem with the very thin films, which were extremely hard to produce using this method. The surface of the resultant film was dull, probably due to the machined surface of the steel discs. The gauge reading the thickness was not accurate at the thicknesses that we were interested in and the exact thicknesses had to be measured for each film by some other method.

Because of the matt surface of the films, the resultant scattering of light at sodium wavelengths precluded the use of the Michaelson interferometer. In order to determine the thickness and uniformity of the resultant films, a solid state detector and a ^{241}Am source were used. The ^{241}Am alpha source, the thin film and the SSD were placed in line inside a vacuum chamber. Several thin films were prepared using the water based method. The Michaelson interferometer was used to determine the thickness and uniformity of each of these films. The chamber containing the films and the SSD was evacuated to a pressure of about 10^{-6} Torr. The pulse height of the 5.49 MeV alpha, after passing through the film, was recorded. The peak position was

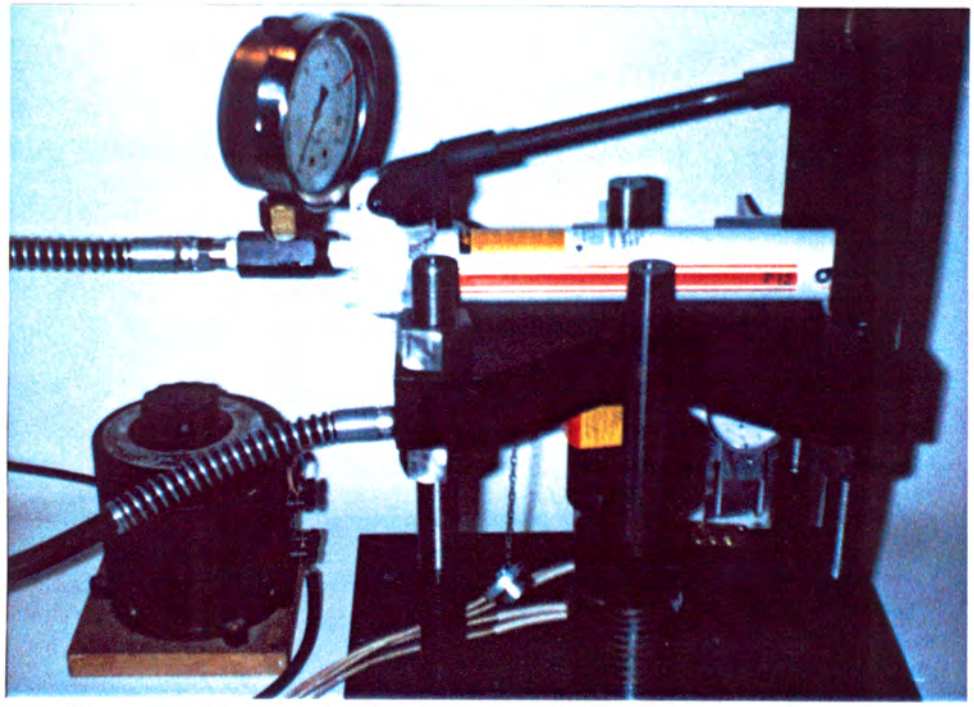

Thin film press, side view, showing variac on left side, pressure gauge (large gauge), thickness gauge (smaller gauge) and piston connected to hydraulic pump (white cylinder).

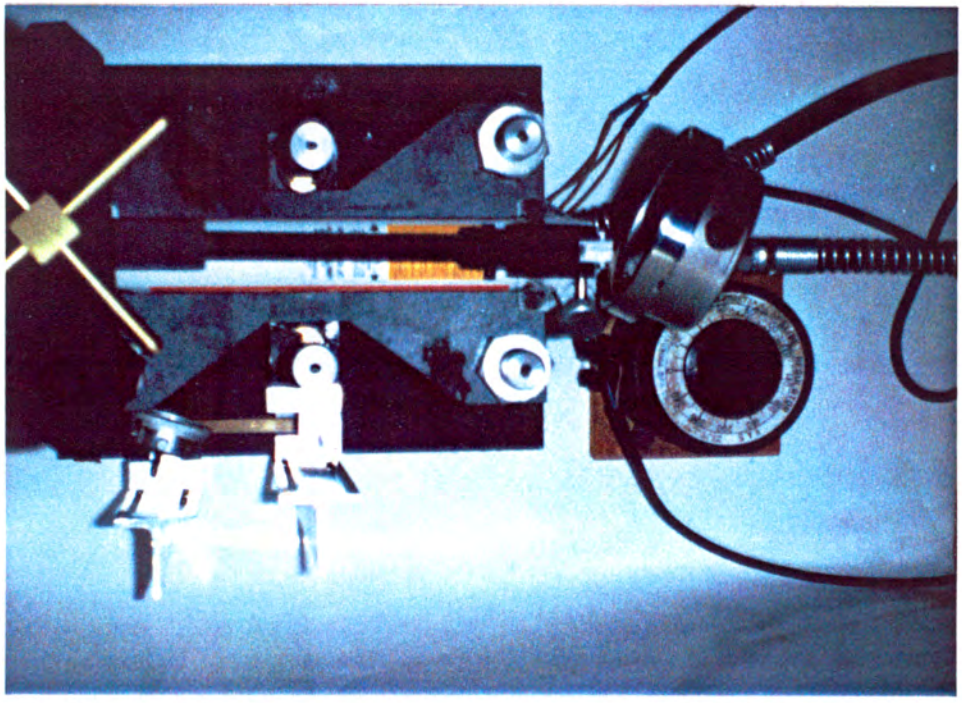

Thin film press, top view.

dependent on the film thickness and the peak width gave an indication of the film uniformity (which was checked optically). In this way, a calibration curve of peak position vs film thickness was obtained for the water based films, and hence the thickness of the pressed film could be determined. The alpha peak width was used as a criterion to decide whether a particular film was of acceptable uniformity. In influence of energy straggling, and subsequent alpha peak broadening, was taken into account when considering the thicker films. The calibration curve is presented in fig 6.

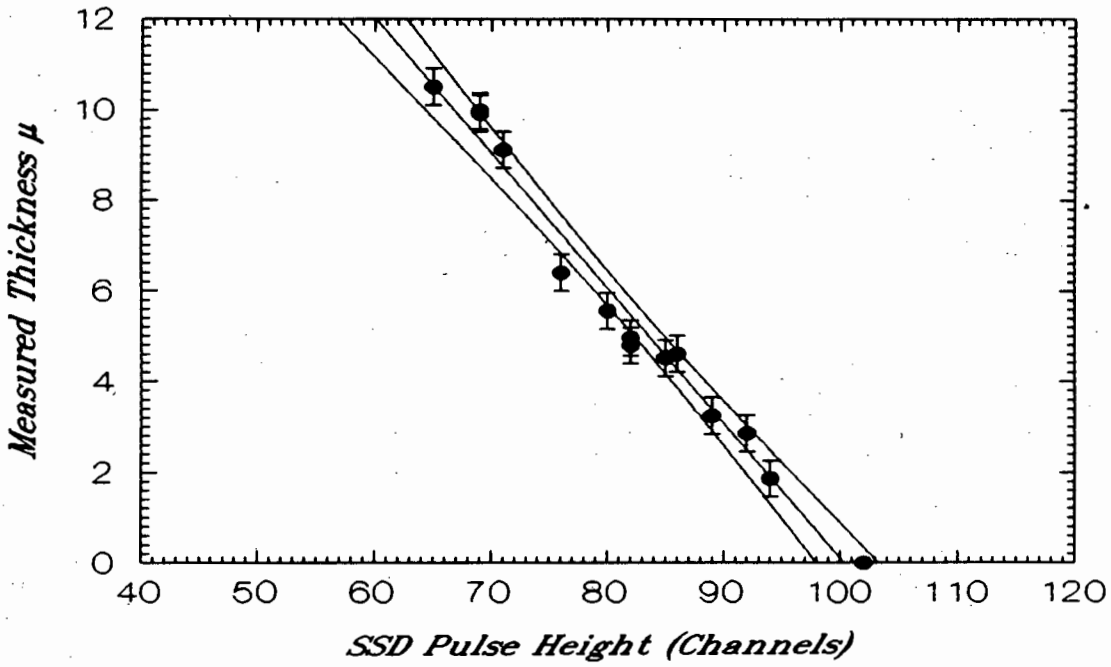

Figure 6. Pressed film SSD calibration curve

A straight line curve was drawn through the data. From this line the function relating the observed pulse height in the SSD to the thickness of the film was

$$T = aPH + b \qquad 10$$

where PH is the pulse height in the SSD. The thicknesses of the pressed films were determined by recording the pulse height of the 5.49 MeV alpha after having passed through the film, and using the calibration curve. The values of the two fitted parameters are

$$a = -0.30 \pm 0.01$$
$$b = 30 \pm 1$$

§4.4 ANNEALED GLASS BASED FILMS

The starting material for this method is the glass based films of §4.2. Once the data collection of the glass based films were completed, the glass disc with the film was removed from the PM tube and all coupling fluid removed from the glass with acetone. The film press was heated to 85°C for the NE102A films and to 115°C for the NE118 films. The glass slide was placed on the press and the gap between the two steel discs reduced to about 1mm between the top steel disc and the scintillator

film on the glass. This arrangement allows the maximum amount of heat to be focussed on the film itself. The glass slide was left for between 5 and 10 minutes to allow the film to melt completely. The heating elements were then switched off and the glass slide with the film allowed to cool, after which it was mounted on the PM tube for data collection. Checking of the thicknesses and uniformity of the annealed films was impossible as these films could not be removed from the glass. Any serious non-uniformity in the annealed films would, however, have shown up in the subsequent spectrum of the film.

§4.5 FILM MOUNTING AND DATA COLLECTION

Once the thin films had been produced by any one of the above methods, they were mounted for data collection. An RCA 8575 photomultiplier tube was used for the recording of the scintillations. The face of the tube was carefully cleaned with acetone and a thin layer of Corning type 52 optical coupling fluid was spread over the surface. The thin film, or glass disc with the thin film on it, was then carefully placed on top of the coupling fluid. The PM tube was placed upright in a vacuum chamber which was evacuated to a pressure of about 10^{-4} Torr. The PM tube was left in the chamber allowing any air that may have been trapped in the coupling fluid to escape. Once this was complete the PM tube was mounted as indicated in the diagram of fig 7.

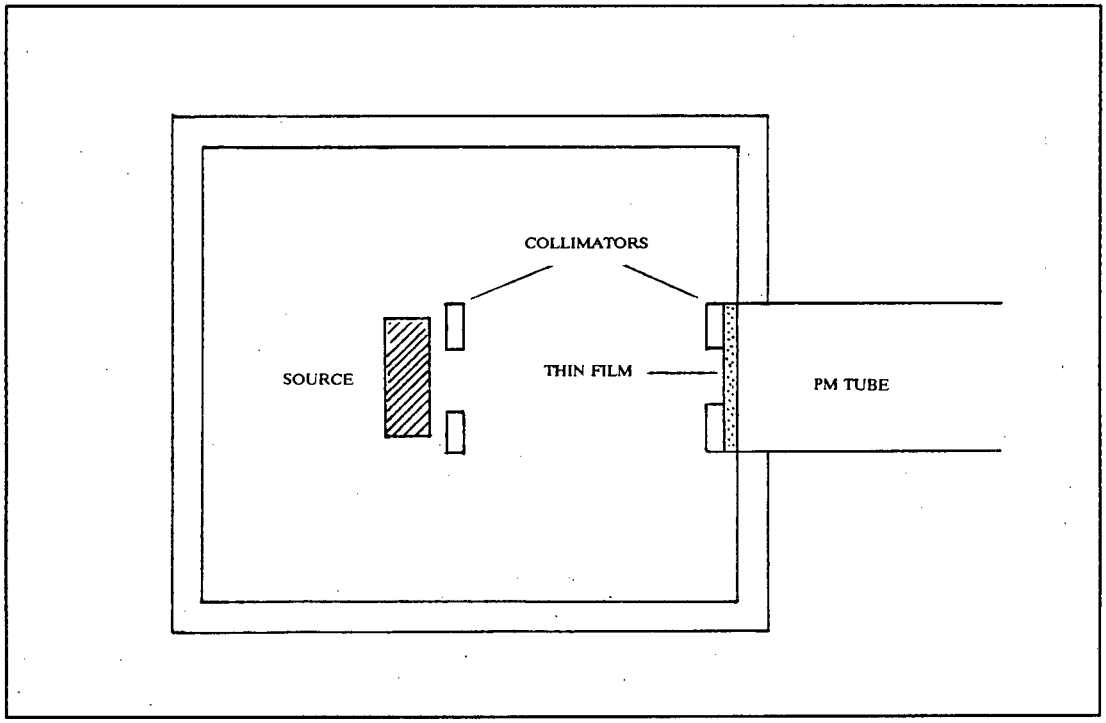

Figure 7. Diagram of setup for recording of data.

A circular collimator of diameter 17 mm restricted the active area of the scintillator. For the pressed films the collimator diameter was 5 mm. The data collection time in this case was increased in order to obtain the same statistics as for the other films. The source used was a ^{252}Cf spontaneous fission source mounted on a nickel disc of diameter 2.5cm and thickness 0.75cm. The source had an activity of 37 kBq, and was collimated with a 17 mm diameter collimator. The source was placed inside an aluminium steel vacuum chamber with dimensions 15cm x 20cm x 12cm. At one face

of the chamber was a hole for the PM tube. The source and PM tube were carefully aligned, with the scintillator a distance of 8cm from the source. The chamber was then evacuated to a pressure of about 10^{-6} Torr. Background readings were taken before the source was introduced and again after it was removed. All spectra collected were corrected for the background. The electronic setup was standard and is shown schematically in fig 8. It consisted of a RCA 8575 photomultiplier tube, a Canberra model 1405 pre-amplifier and an Ortec 572 amplifier in series. One branch of the signal from the amplifier was used to gate the 8-parameter interface, and the other branch was sent to a Canberra 8075 analog-to-digital converter via a Ortec 427A delay amplifier with a 3.5 μsec delay. The 8-parameter interface was used to provide the gate for the ADC. A BBC microcomputer was used to record the data, which was received from the ADC via the 8-parameter interface.

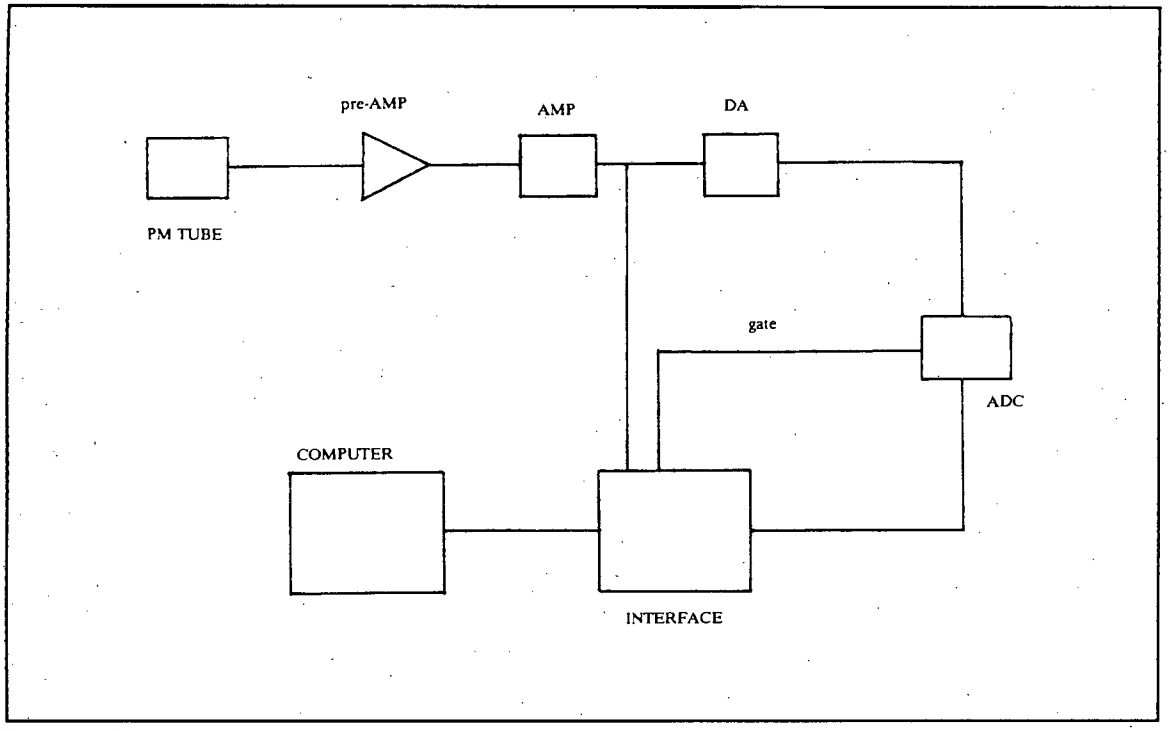

Figure 8. Electronic setup for recording of data

§4.6 DATA PROCESSING

Figure 9 shows the complete spectra of the water based NE118 10.64 μm thin film prior to data analysis.

The data was recorded as number of counts versus channel number, and were smoothed using a fast fourier transform method (Flannery et. al[58,59]). The smoothed FFT curve is shown superimposed on the raw data in figure 9. A function which consists of the sum of two Gaussians was then fitted to the data. The function is of type

$$F(x,y) = A\exp\left(\frac{-(x-B)^2}{2C^2}\right) + D\exp\left(\frac{-(x-E)^2}{2F^2}\right) \qquad 11$$

where the variables A through F are fitted variables with the peak positions, peak heights and half widths of the smoothed FFT curve the initial estimates of A through

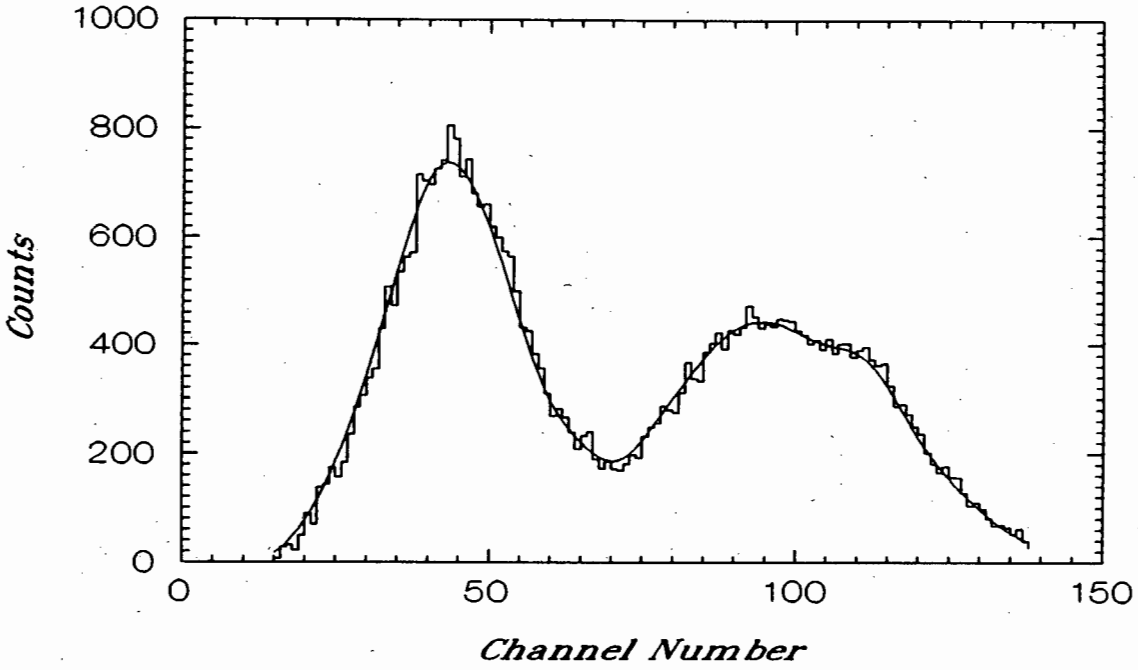

Figure 9. NE118 10.6 μm water based thin film with FFT transform.

F in the best fit of equation 11. Since the double Gaussian function fitted the data so well, this function was used on all the data. This has the further advantage that the peak positions and the errors on these positions could be obtained analytically, something that was not possible with the FFT method. These errors on the peak positions are given by

$$\Delta P = \frac{\sigma}{\sqrt{N}} \qquad 12$$

where N is the total number of counts under the peak, and σ the standard deviation. Typical errors were 0.05-0.20 channels. Figure 10 shows the same spectra as in fig 9, but with the fitted gaussian function superimposed over the data.

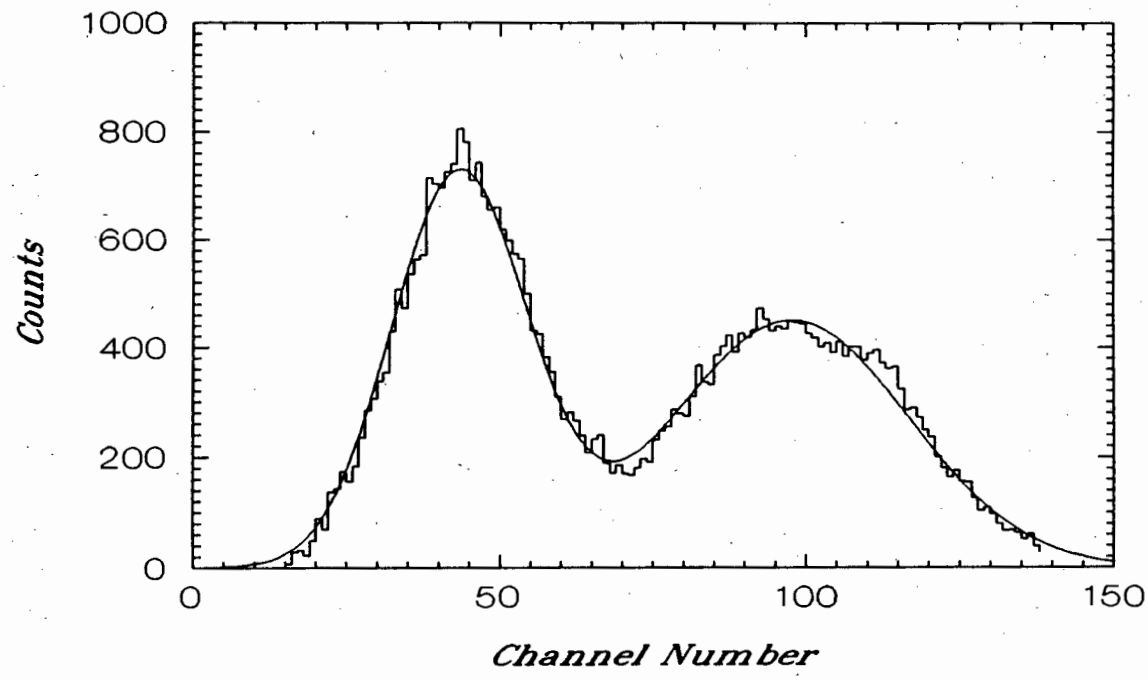

Figure 10 NE118 10.6 μm water based film, with fitted function of equation 11.

§5 DATA ANALYSIS

This chapter contains all the measured data as well as expressions for their predicted behaviour. In the case of the non-annealed glass based thin films it also provides a model for the observed behaviour.

§5.1 PREDICTED LUMINESCENT BEHAVIOUR

The differential luminescence dL/dx of a thin film of scintillator is proportional to the differential energy loss dE/dx of the incident particle. In order to take account of surface and saturation effects, semi-empirical relations for the expected dL/dx versus dE/dx behaviour of charged particles in scintillators were developed by Birks and Chou (§2.5). The so-called Birks relation is given by

$$\frac{dL}{dx} = \frac{A\frac{dE}{dx}}{1 + kB\frac{dE}{dx}} \qquad 1$$

where k is a quenching parameter, and A and B are fitted constants. Chou's relation is given by

$$\frac{dL}{dx} = \frac{A\frac{dE}{dx}}{1 + B\frac{dE}{dx} + C(\frac{dE}{dx})^2} \qquad 2$$

where A,B and C are fitted constants. The fitted constants A and B are the same for the two relations. In the limit of small dE/dx the two relations reduce to the form

4

For small energy loss, surface quenching effects (§2.4) will reduce the expected L value, and for large energy loss, saturation of the luminescent centres (§2.4) will lead to saturation of the L response. The linear relation of equation 6 should describe the luminescent response of heavily ionising particles quite accurately. In order to obtain a semi-empirical expression in terms of our measured variables an expression for the energy loss, ΔE versus the distance travelled in the plastic T, of the fission fragments is required.

The stopping of fission fragments shows considerable differences from the stopping of light ions (Serge[38]). For almost its entire range in the stopping material the alpha or proton maintains a constant charge. The capture and loss of electrons is important only toward the very end of the range. For a fission fragment, however, the initially large positive charge is continuously being reduced by the capture of electrons in the slowing down process (Bell[39]). This has a marked effect on the mechanism for the energy loss of the fragment toward the end of its range. In this region collisions between the fragment and the nuclei of the stopping material are more important than the electronic excitation process. The relation often used to describe the differential energy loss of fission fragments is due to Bohr[40] .

$$\frac{dE}{dx} = \frac{4\pi e^4 N}{mV^2}(Z_1^{eff})^2 \ln\left(\frac{1.123mv^3}{\omega e^2 Z_1^{eff}}\right) + \frac{4\pi e^4 N}{M_2} V^2 Z_1^2 Z_2^2 \ln\left(\frac{M_1 M_2 V^2 a_{12}^{scr}}{M_1 + M_2 Z_1 Z_2 e^2}\right) \quad (13)$$

where e is the electron charge, N the number of absorber centres per unit volume, m the mass of the electron and V the velocity of the fragment. Of most concern is the parameter, Z^{eff}. This is the instantaneous effective charge that the fragment has as it transits the stopping material, and is a function of several parameters, such as initial charge of the fragment and the fragment velocity (Fulmar and Cohen[41]). While progress has been made in determining relations for Z^{eff} in gases, no relation exists for this quantity in plastics. For this study a semi-empirical approximation of E versus x was made. Fulmar[42] has undertaken the measurement of the range of fission fragments in various absorbers. In all the cases it is possible to fit a second order polynomial to the residual energy-distance in absorber data and obtain a very good fit. Figure 10 shows the result of fitting a second order polynomial to the data of Fulmar[42]. In this case the absorber is Al and the incident fission fragments are the mean heavy fragment from neutron induced fission of ^{235}U.

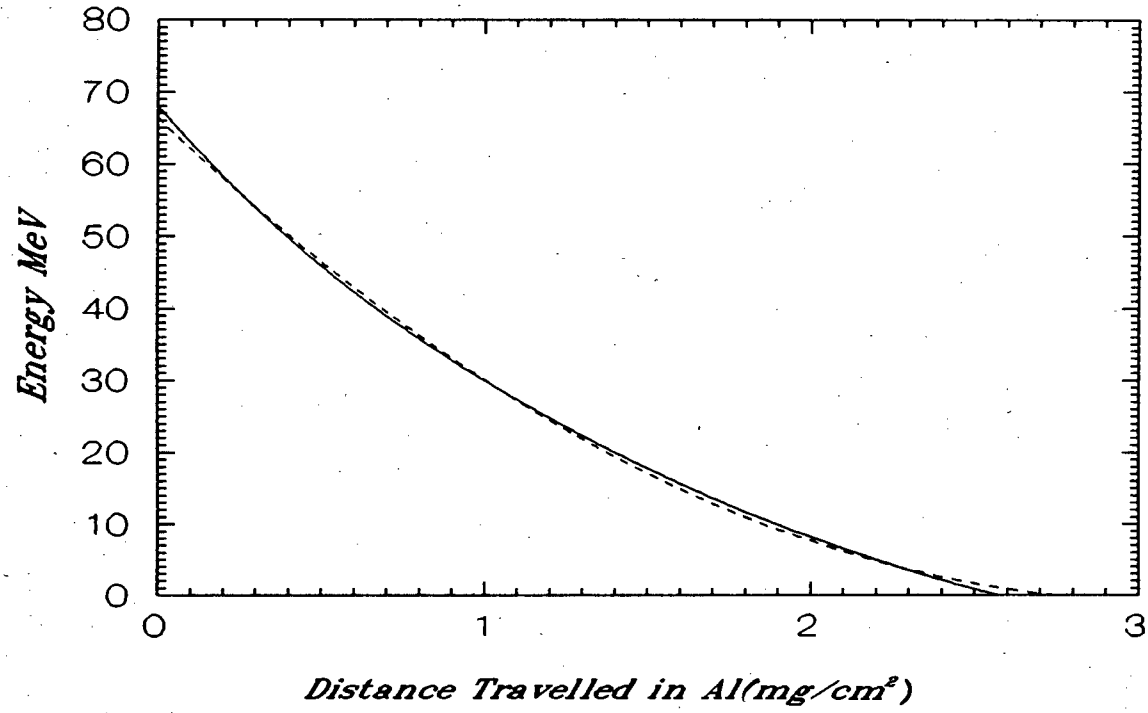

Figure 11. Energy vs Distance travelled in Al relation for neutron induced fission of ^{235}Uranium (solid line) with fitted polynomial (dashed line), from Fulmar[42].

The solid line represents the data of Fulmar, and the dashed line , the second order polynomial. The particle energy E as a function of distance travelled in the plastic by the fission fragment T, is then approximately given by

$$E(T) = \alpha T^2 + \beta T + \gamma \quad (14)$$

Although the absolute values of the constants are not required as we need only the form of the E versus T relation, we have derived the values of the constants for the

mean light and heavy fragments in NE102A for completeness. The data of Whetstone[43] were used to obtain the average energy and mass of the mean light and heavy fragments of ^{252}Cf, and the work of Fink[44] was used to obtain the initial charges of the two fragments. With these data, the range energy tables of Northcliff and Schilling[45] were consulted to obtain the range of the light and heavy fragments in the two plastic scintillators. The range of the two fragment groups are shown below

$$R_{light} = 18.7\ \mu m$$
$$R_{heavy} = 15.6\ \mu m$$

The values for the fragments in NE118 are about 1.5% larger. Using equation 19 and the total energy and range of the fragments, E(T) functions were prepared by setting E(0 μm) = 80.0 MeV, and E(15.6 μm) = 0 MeV for the mean heavy fragments and solving the simultaneous equations

$$80 = A(0)^2 + B(0) + C$$
$$0 = A(15.6)^2 + B(15.6) + C$$

The function for the light fragments was prepared in a similar fashion, setting E(0 μm) = 105.7 MeV and E(18.7 μm) = 0 MeV. The forms of these two energy versus distance travelled in plastic functions are shown below, where T is in μm and E in MeV.

$$E(T)_{heavy} = 1.40x10^{-3}T^2 - 5.15T + 80.0$$
$$E(T)_{light} = 6.85x10^{-3}T^2 - 5.78T + 105.7 \qquad 15$$

Using the expression for luminescence in the limit of small dE/dx, equation 6, and extending it to fission fragments, we have substituted equation 14 and simplified, giving an expression for the predicted L versus T behaviour in the limit of small dE/dx.

$$L(T) = \acute{A}(\alpha T^2 + \beta T + \gamma) + L_0 \qquad 16$$

which reduces to

$$L(T) = AT^2 + BT + C \qquad 17$$

where T is film thickness, and A,B and C are fitted constants. The parameters A,B and C are given by

$$A = \acute{A}\alpha$$
$$B = \acute{A}\beta$$
$$C = \acute{A}\gamma + L_0$$

The parameters A and B determine the shape of the L versus T curve, while C determines the height of the curve. In order to satisfy the condition that the shape of the scintillation curve be the same for the four methods, A and B was fixed at the same value, and C was allowed to vary across the four methods of preparation. The expression does not take surface quenching effects into account, and will thus

overestimate L for the very thin films. It must be pointed out that the preceding analysis relies on the assumption of small dE/dx for fission fragments in plastic. This assumption may not be valid and the apparent good fit of equation 17 to the data (e.g. fig 12), does not necessarily confirm the correctness of the assumption of small dE/dx, since the fit was tested over a small thickness range only.

§5.2 NE102a and NE118 DATA

All the data for the two types of film (NE102a and NE118) and for the various methods of preparation of the films are presented in figures 11-18, where the peak positions for the heavy and light fragments , respectively, are plotted as a function of film thickness. In all cases the heavy fragments are plotted as triangles and the light fragments as circles.All the curves vary smoothly with film thickness except the one for the (fig. 13 and 17) glass based films for both NE102a and NE118. In these two cases there is a marked step in the curves at film thicknesses round about 5 μm. The step occurs for both the light and heavy fragments in each case. We have fitted the smooth curve of equation 22 to all the data not showing the step like behaviour. This equation can obviously not be valid for thicknesses $T \rightarrow 0$. The response must drop to zero as T is made very small, mainly because of surface quenching which is expected to become marked for $T \leq 3$ μm. The fits are in general quite good. The adjusted parameters A and B are as follows.

	A_{light}	A_{heavy}	B_{light}	B_{heavy}
NE102a	-0.42	-0.15	9.25	3.25
NE118	-0.29	-0.28	8.09	6.12

The corresponding values of C can be obtained from the curves at T=0. Evidence for surface quenching may be seen in figures 11,12 and 14 where, for NE102a, the experimentally determined response falls below the fitted curves for $T \leq 4$ μm. This effect does not show for NE118 (figures 15,16 and 18). As mentioned above, the experimental points must depart from the smooth curve for small T and it may be that surface quenching for NE118 sets at a lower value of T than for NE102a. It should be noted that the step occurs at $T \approx 4$ μm for NE118 (fig 17) whereas it occurs at $T \approx 5$ μm for NE102a (fig 13). The step-like behaviour of the non-annealed glass based films was also observed by Brooks and McLeod for NE102a. We have now confirmed their results and have shown that it occurs for NE118 as well. The effect is not a surface quenching effect since it does not occur for the water based films of for pressed films. It can therefore be concluded that the step-like behaviour is associated with the glass-scintillator interface.

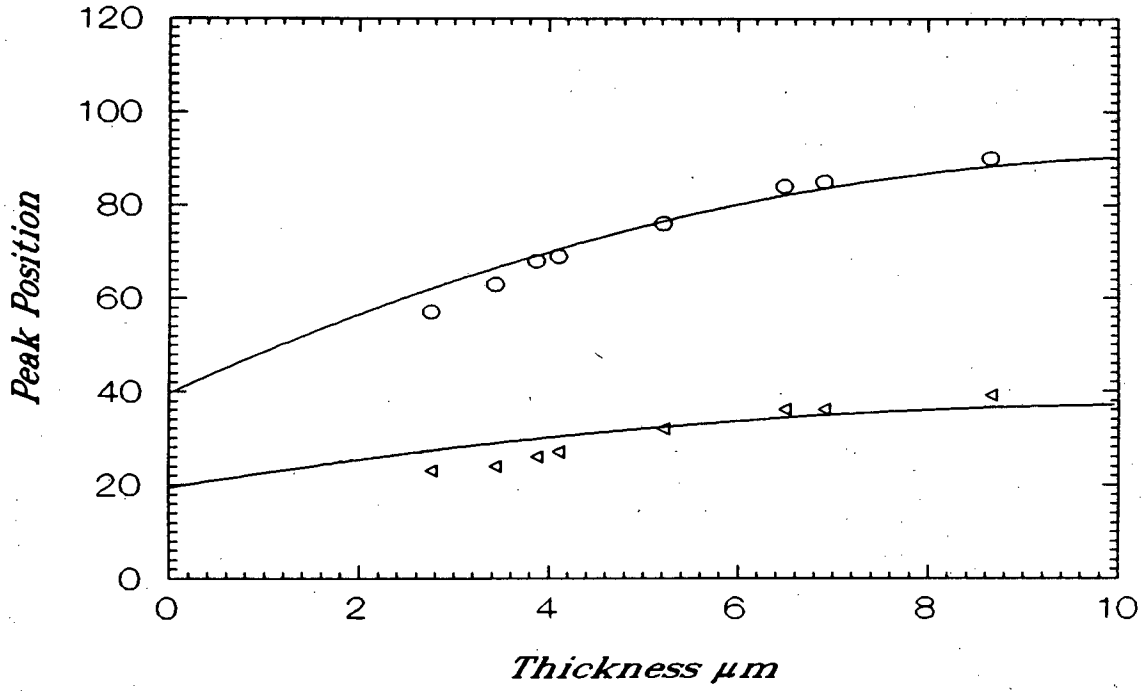

Figure 12. L versus T response of NE102A water based films.

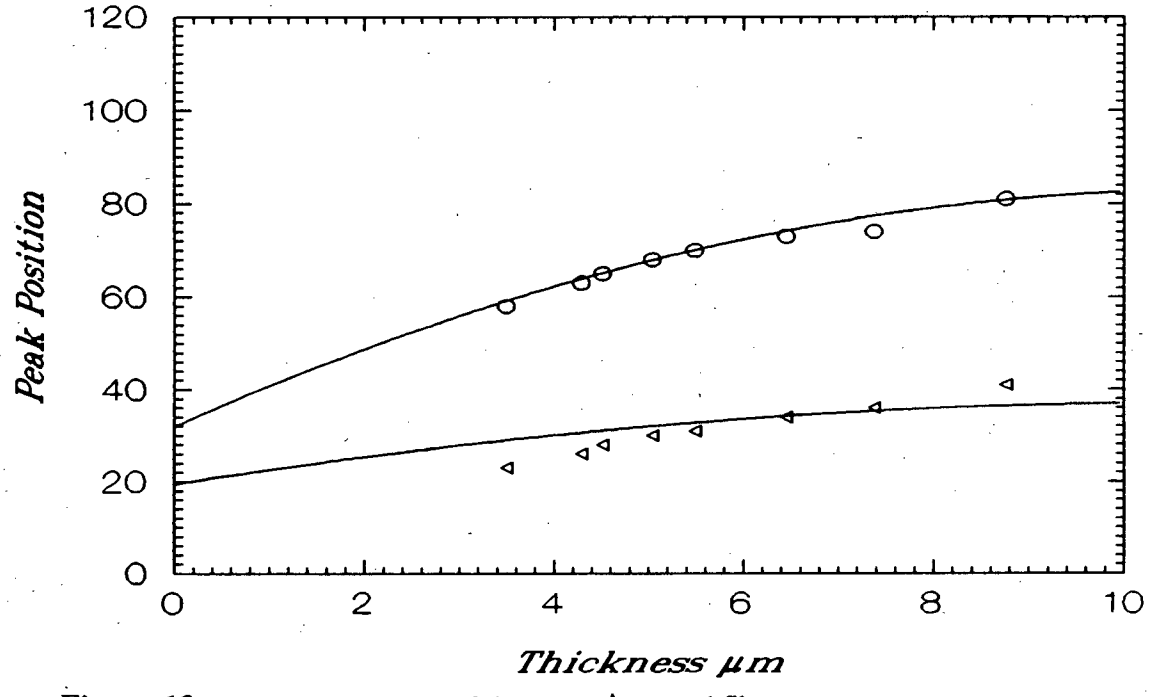

Figure 13. L versus T response of the NE102A pressed films.

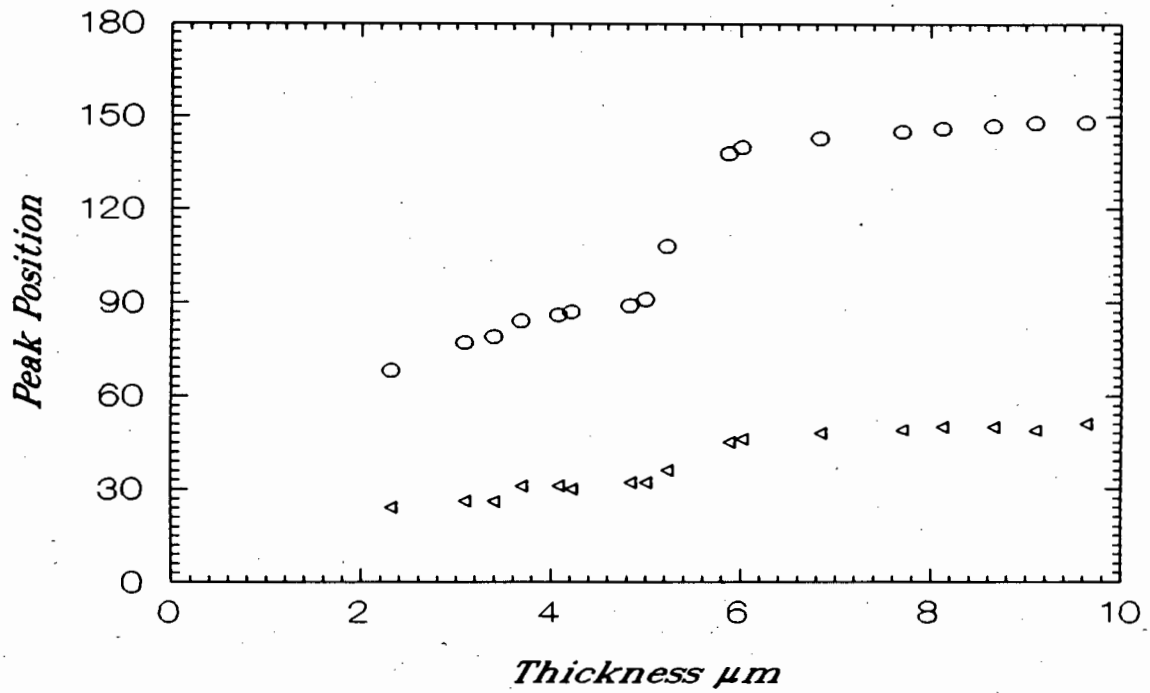

Figure 14. L versus T response of NE102a non-annealed glass based films.

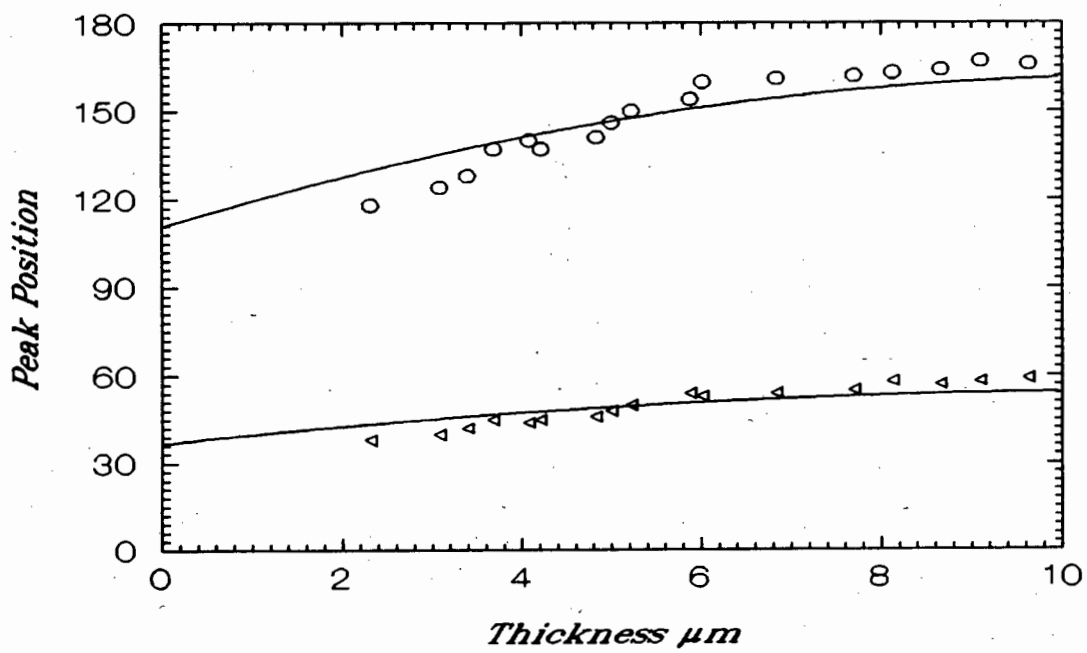

Figure 15. L versus T response of NE102a annealed glass based films.

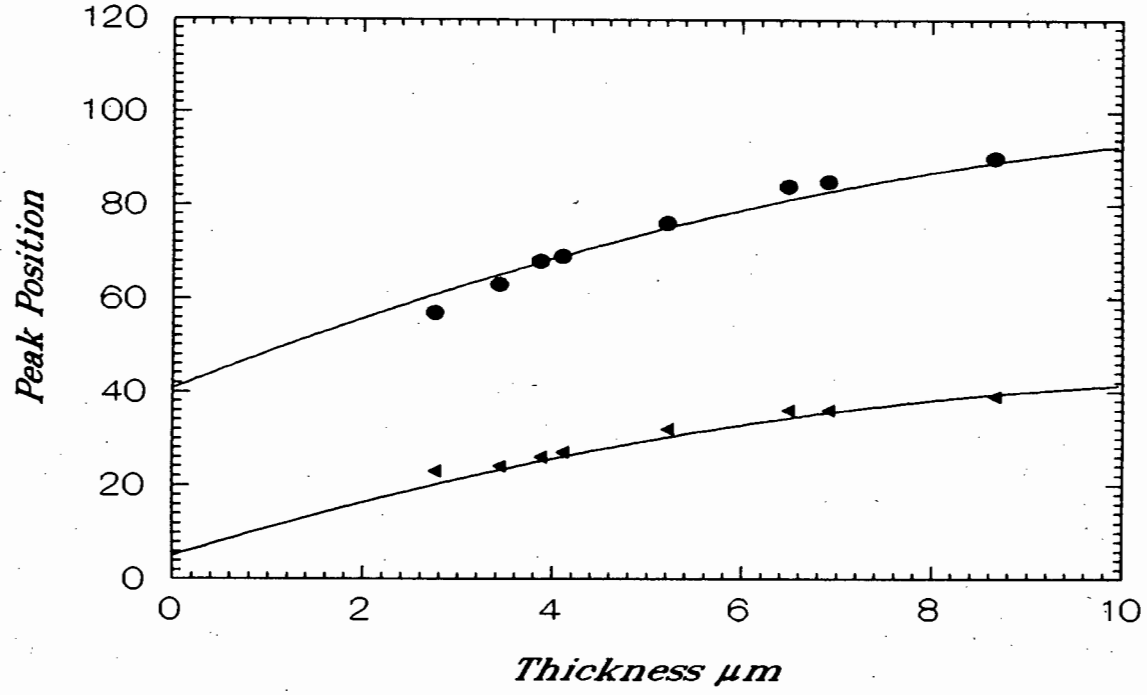

Figure 16. L versus T response of NE118 water based films.

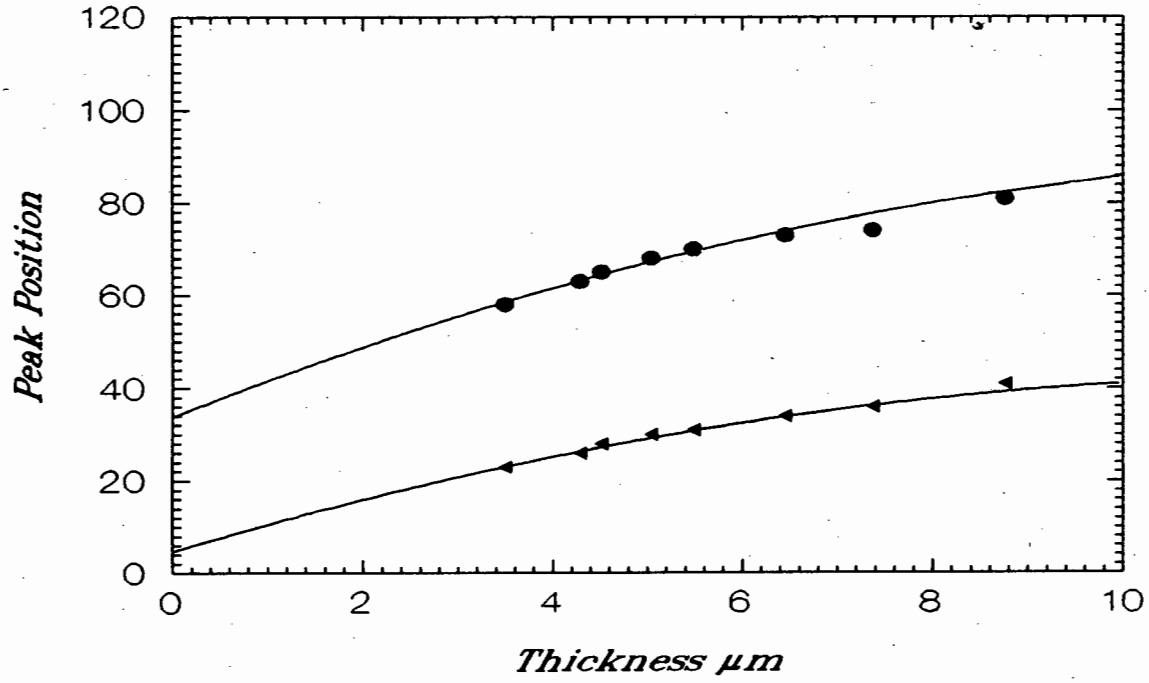

Figure 17. L versus T response of the NE118 pressed films.

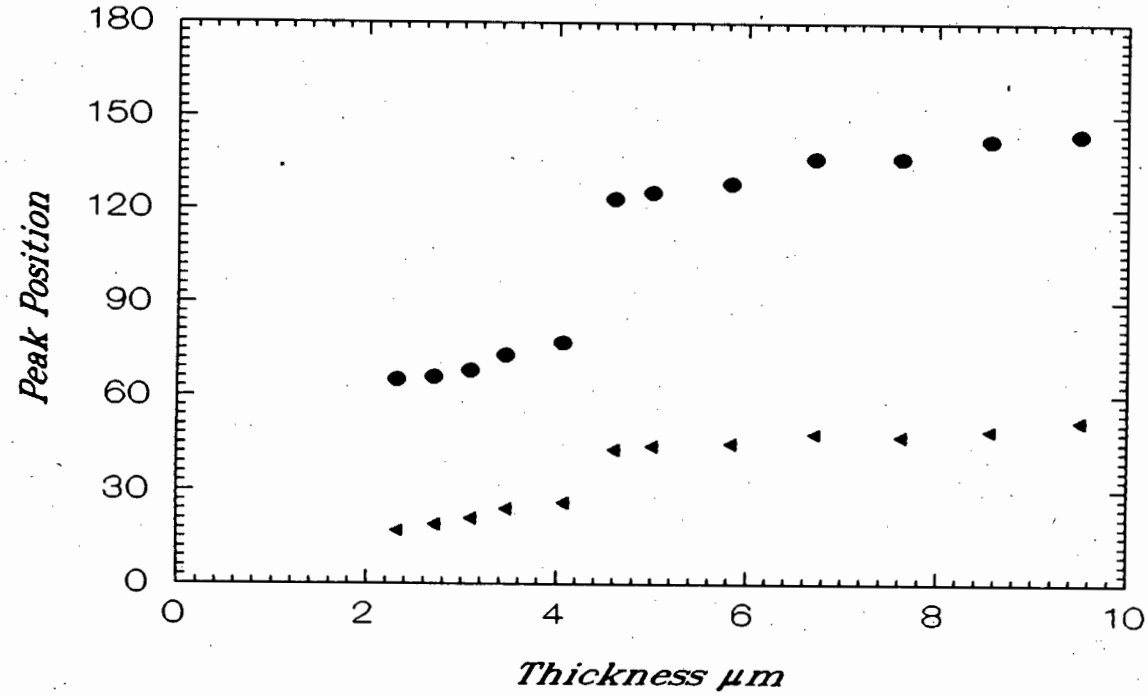

Figure 18. L versus T response of NE118 non-annealed glass based films.

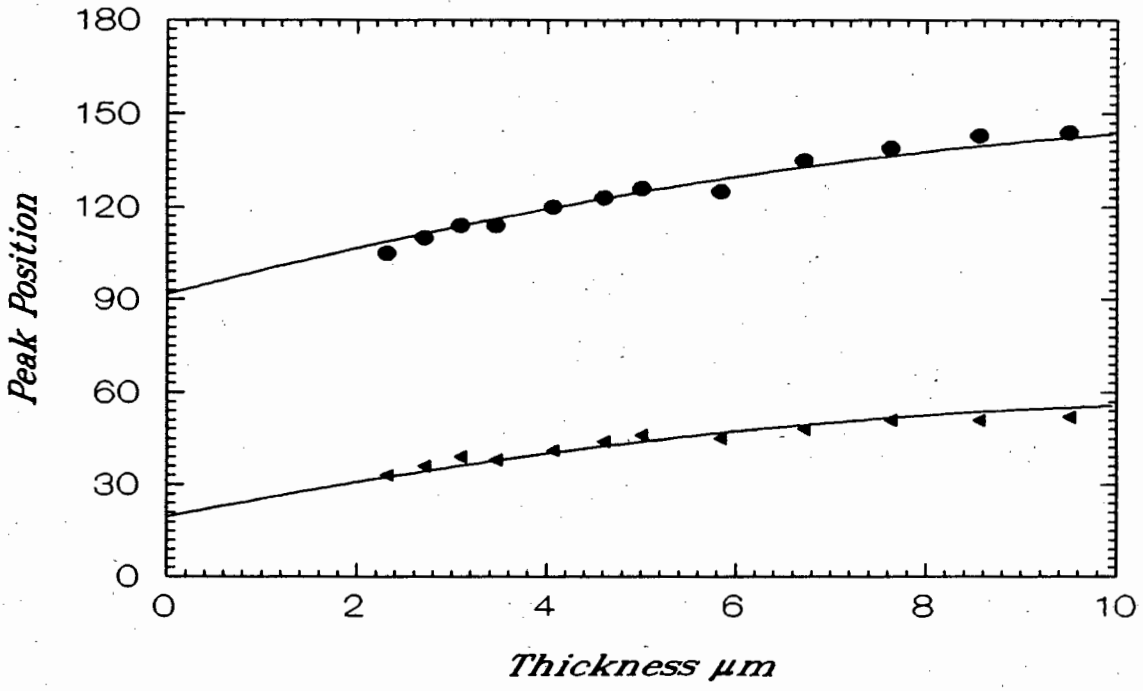

Figure 19. L versus T response of NE118 annealed glass based films.

§5.3 *INTERFACIAL PHENOMENON*

A detailed description of the solid-liquid interface is included in this section because the striking results of our investigation are obtained for films that were prepared with such an interface. The detail that follows will become important as they provide a very significant body of evidence that will be used to account for the behaviour seen in the glass based films. The significant point about the solid-liquid interface is that the presence of the solid leads to the orientation of the liquid molecules lying above it.

Derjaguin[60] was among the first to provide results on the effect of surfaces in liquids. He reported that a liquid film in contact with a glass or mica surface was ordered to a depth of 0.15 μm. Direct evidence of deep surface orientation has been found by several workers. Optical anisotropy in homogeneous liquids is evidence of molecular orientation. Taylor and King[61] found optical anisotropy in long chain fatty acids to a depth of 0.4 μm when the fatty acids were placed on a glass surface. Adsorption of a liquid layer, where the layer is thicker than a monolayer, from a saturated vapour onto a surface is evidence of the forces extending from the solid, and from one molecule to another, into the liquid. This mechanism of relayed action and long range effects of surface forces was first suggested by Hardy[62]. Experimental evidence for this was found by Lenher and McHaffie[63], and Lenher[64], who exposed various plane surfaces to atmospheres nearly, but not quite, saturated with water or benzene vapour. Films of definite limited thicknesses were obtained. Lenher's films were calculated by Joris and Taylor[65] to be 18 to 62 monolayers thick. The work indicated that the thicknesses of the resultant films were dependent on the surface used and on the type of liquid deposited on the surface. Bangham[66] reported that deposition occurred to only a definite distance from the solid surface, indicating that the surface effect had a definite range in the liquid. Studies of electron diffraction also provide direct evidence for the existence of a surface layer. Brummage[67] found a disorientation temperature up to which the film gave a pattern by electron diffraction, indicating some order in the structure. Above the disorientation temperature, the ordered structure was lost. His work showed that for long chain molecules, the surface effect extended up to the order of micrometers, possibly due to the size of the molecule. Another conclusion that is reinforced from this study is that the range of the surface forces is dependent on the number of monolayers and not only on the absolute distance. Work by Mcbain[68] provided evidence that the surface effect seen is applicable to 2 component solutions, and not merely homogeneous liquids. Less striking evidence for the existence of a surface layer in a liquid also exists. Watson and Mellon[69] studied the conductance that was reported to occur in thin films of oils. They found that whatever the nature of the change in the oil that had occurred, it could be ascribed to the presence of surface forces. Wilson[70] reported that in all cases the conductivity of the thin oil film was very high, or metallic, and appeared suddenly as the film was made thinner. Work on the friction coefficient for alcohol between steel surfaces was carried out by Bowden[71], who reported that the coefficient was negligible for thicker films but rose rapidly when the thickness was reduced below 0.36 μm. These works indicated that by reducing the thickness of a film, a sudden onset of unusual properties occurs, due to the presence of the surface. Local increases in viscosity in the immediate region

of a solid surface can be explained in terms of strong forces extending from the solid surface deep into the liquid. Results by Shereshefsky et. al[73]. and Duff[72] on the vapour pressure and viscosity of liquids in capillaries suggested that the capillary wall was capable of inducing changes in the liquid structure over distances of the order of a micrometer. Henniker$_{66}$ in his review noted that a solid surface in contact with a liquid, has the effect of determining the structure of a solid that forms from the liquid. Work by Rothen[74,75], on organic hydrocarbons and antigens, showed that induced surface orientation in a liquid can be transferred to a solid that grows from that liquid. Rothen[76] later reported the same kind of effect with an enzyme. His work provided evidence that the surface effect seen in a liquid placed on a solid surface can affect the resultant solid derived from that liquid. Bradley[77] reported a similar effect in inorganic crystals crystallized out of solution. Finch[78] found that the structure of nickel crystallized on copper, follows that of copper up to a thickness of 3 μm. The work of Rothen, Finch and Bradley provides evidence that the presence of a surface changes the structure of a liquid layer above it, and that when such a liquid layer solidifies, such structural changes are transferred to the solid.

Reviews on the subject of surface depth in liquids can be found in McBain[79], Henniker[66] and Adamson[80]. From the above body of experimental evidence and theoretical postulates we can conclude that the forces at the surface of a solid are long range in nature, and normal to the direction of the surface.

§5.4 A MODEL FOR THIN FILM STRUCTURE

A careful consideration of the liquid solution before it solidifies on the glass will allow an approximation of the physical structure of the resultant film. The glass surface has associated with it a surface orienting force (§5.3) the direction of which is normal to that of the surface, and which extends into the liquid layer above the glass. The surface orienting force has a definite range α in the liquid. We will consider two cases, films thinner than α, and films thicker than α. For films thinner than α, the entire thickness of the liquid layer that solidifies to become the film is within range of the surface orienting force. The individual molecules of the liquid become aligned by the force along a general direction normal to the glass surface, forming an ordered structure of molecules. As the one component of the two part solution is preferentially adsorbed and the film solidifies, the surface orienting force ensures that the solid structure has the same ordered nature, with the molecular chains having a general direction normal to the surface (Henniker, Rothen).
Thus for films thinner than α the entire film will consist of this ordered surface region.

If the films are thicker than α, then the range of the surface orienting force no longer extends across the entire thickness of the film. For the portion of the liquid layer above α, beyond the range of the surface orienting force, the molecules will adopt the normal random configuration. Films thicker than α will then consist of two regions; an ordered surface region, and a random "bulk" region. The molecules in the ordered arrangement of the surface region will have a higher potential energy compared to the random arrangement of the bulk. The molecules at the boundary of the surface region in the liquid, will feel less of the surface orienting force due to

the shielding effect of the underlying molecules. These molecules will not be held in the ordered array as firmly as the molecules near the glass surface. It will be energetically favourable for these molecules to overcome the surface orienting force and adopt the random configuration of the bulk region lying above it. As molecules adopt the random configuration at the boundary of the surface region, it will become more difficult for the molecules left in the surface region to do likewise since they are nearer the glass surface and feel the surface orienting force more strongly. At some distance $r < \alpha$, the molecules will be unable to overcome the surface orienting force and will remain in the surface arrangement. Hence the presence of the bulk material above the surface layer before the film solidifies, results in the surface layer being reduced in thickness. The film prepared on the glass will thus have two configurations; for thicknesses below α the film will be all surface region, and for films thicker than α the films will consist of two parts, a random bulk region and an ordered surface region, where the thickness of the surface layer will be $< \alpha$.

The physical and other properties of such a surface layer will be different from that of the bulk. Of most interest are possible changes in the scintillation efficiency of the surface layer relative to that of the bulk. The scintillation efficiency of a material is dependent on the effectiveness of the process of energy transfer from the bulk constituent to the scintillating molecules (§2.5). In plastics, this transfer takes place predominantly via a non-radiative dipole-dipole mechanism that is accurately described by Forster kinetics (§2.3). This energy transfer is inversely proportional to the sixth power of the critical transfer distance R_0. If ϵ is the overall scintillation efficiency of the material, then

$$\epsilon \propto \frac{1}{R_o^6} \qquad 18$$

Because of the nature of the dependency, very small changes in R_0 will result in significant changes in ϵ. R_0, by its nature being a non-radiative transfer distance, will depend on the internal structure of the material, and an ordered array of molecules will have a different R_0 from that of a random arrangement of molecules. The scintillation efficiency of the surface region will be different from that of the bulk region. In order to estimate how the surface layer varies with film thickness above α, we can look at Kwei's work on the Young's modulus of polystyrene with transcrystalline surface layers (§3.4). His work indicates that a good approximation may be a curve where some property (like Young's modulus in his case or perhaps absolute surface layer thickness in our case) changes exponentially with thickness, reaching some saturation value beyond a certain thickness (fig 4). If we take T_s as the absolute thickness of the surface layer, T as the total thickness of the plastic film, and T_c as the maximum thickness at which the film is all surface layer, then it is proposed that the surface layer varies with film thickness T, where $T > \alpha$, as

$$T_s = (T_c - T_o)\exp(-\kappa(T - T_c)) + T_o \qquad 19$$

where T_0 is the thickness toward which the surface layer tends for thicker films, and κ an empirical constant. Figure 20 shows a plot of the proposed variation of the surface region T_s with total film thickness T. The parameter values used are arbitary.

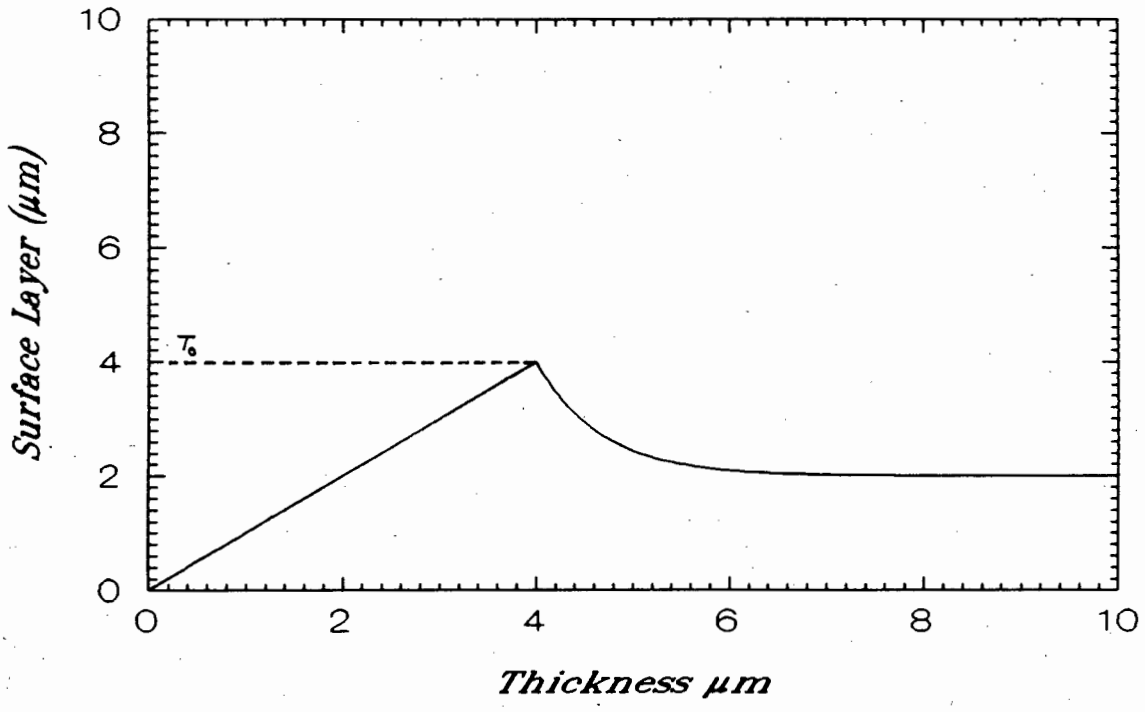

Figure 20 Proposed variation of the surface layer with overall film thickness T

Using equations 17 and 19 we can derive a semi-empirical relation for the expected L versus T behaviour of the non-annealed GBF. The luminescence of the surface region in the absence of the bulk is given by

$$L_s(T) = A_s T^2 + B_s T + C_s \qquad 20$$

The luminescence of the bulk region in the absence of the surface region is

$$L_b(T) = A_b T^2 + B_b T + C_b \qquad 21$$

In that part of the film where both regions are present the total luminescence of the film will be the sum of the fractional contributions of the luminescence of the surface and bulk regions. The overall luminescence of the film will then be

$$L(T) = \frac{T_s}{T} L_s(T) + \frac{T-T_s}{T} L_b(T) \qquad 22$$

substituting the previous equations,

$$\begin{aligned} L(T) &= \frac{T_s}{T}(A_s T^2 + B_s T + C_s) + \frac{T-T_s}{T}(A_b T^2 + B_b T + C_b) \\ &= A_b T^2 + B_b T + C_b + \frac{T_s}{T}[(A_s - A_b)T^2 + (B_s - B_b)T + (C_s - C_b)] \end{aligned} \qquad 23$$

putting $A_s = A_b = A$, and $B_s = B_b = B$, and simplifying

$$L(T) = AT^2 + BT + C_b + \frac{T_s}{T}(C_s - C_b) \qquad 24$$

the reasons for the above conditions will become clear later. If $C^* = C_b - C_s$, then the total luminescence of the film becomes

$$L(T) = AT^2 + BT + C_b - \frac{T_s C^*}{T} \qquad 25$$

substituting the expression for T_s

$$L(T) = AT^2 + BT + C_b - \frac{C^*(T_c - T_o)}{T}\exp(-\kappa(T - T_c)) - \frac{C^* T_o}{T} \qquad 26$$

putting

$$\eta = \frac{C^*(T_c - T_o)}{T}$$

$$\acute{C} = C_b - \frac{C^* T_o}{T}$$

into the equation, it reduces to

$$L(T) = AT^2 + BT + \acute{C} - \eta\exp(-\kappa(T - T_c)) \qquad 27$$

which is then the final expression for the luminescence of the film above the critical thickness T_c, where the film consists of two regions, a surface region and a bulk region. Below the critical thickness T_c, the film consists of all surface and the expression for the luminescence is as in equation 25. The overall expression for the luminescence of the film as a function of the film thickness is then the two part function

$$\begin{aligned} L(T) &= AT^2 + BT + \acute{C} - \eta\exp(-\kappa(T - T_c)) \quad T > T_c \\ &= A_s T^2 + B_s T + C_s \qquad\qquad\qquad\qquad T \le T_c \end{aligned} \qquad 28$$

The need for requiring $A_s = A$, and $B_s = B$ now becomes clear. If there are no surface layers, then the total luminescence function must be given by an expression similar to that of equation, 17, a continuous function. In the above two part function, putting $\eta = 0$, and $T_o = 0$ ensures that to satisfy the above condition we must have that $A_s = A$ and $B_s = B$, the condition that was imposed earlier. The overall expression for the luminescence of the film as a function of the film thickness is thus

$$\begin{aligned} L(T) &= AT^2 + BT + \acute{C} - \eta\exp(-\kappa(T - T_c)) \quad T > T_c \\ &= AT^2 + BT + C_s \qquad\qquad\qquad\qquad T \le T_c \end{aligned} \qquad 29$$

The parameters A, B, C, C_s, η and κ are parameters that are varied to fit the data. Figure 21 shows the behaviour of the semi-empirical function for the total luminescence of the thin film prepared on the glass base.

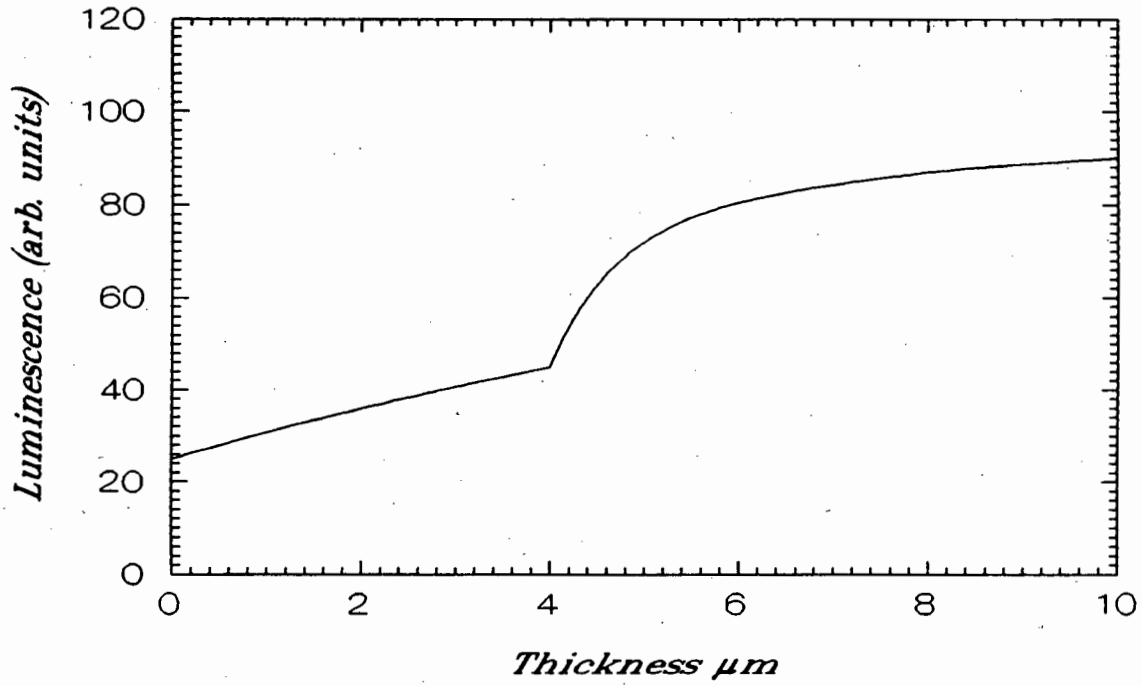

Figure 21 Behaviour of the semi-empirical equation for the total luminescence of the thin films.

While surface layers do exist in polymers (§3.5), such layers are temperature sensitive, and while surface layers can form from melt crystallized polymers on metal or other surface, conditions not easily produced are required. The greatest force countering the formation of surface layers in polymers formed from the melt, is the viscosity of the molten polymer. In normal circumstances we expect that heating a film that has a surface layer will result in the polymer in the melt taking on a random or non-structured configuration, and solidifying in such a configuration, losing all trace of a transcrystalline surface layer. If we take the non-annealed glass based films and subject them to heating (annealing them), then the surface layers should disappear and the film should then behave as it would normally be expected to, i.e. without the luminescent step. If the scintillation efficiency of the surface regions is poorer than the bulk, then on heating, a film with thickness $< T_c$ should show a rise in the total luminescent response compared to before annealing. For films thicker than T_c there should also be a rise in the total luminescent response, but this rise will be much smaller than for films thinner than T_c. This is because the surface layer in these thicker films is thinner than T_c. The function that describes the response of the films after annealing should also be continuous, without any trace of the luminescent step. The response of films should follow the predictions of the equation for the $L_b(T)$, the luminescence of the bulk material. This will fix the parameters A and B in the equation at the same values as they had for non-annealed GBF. Figure 22 shows the expected behaviour of the luminescent response before and after annealing. The parameters have been chosen so that the behaviour of the films can be illustrated. The difference between the luminescence of the annealed and non-annealed films both above and below T_c is thus arbitrary.

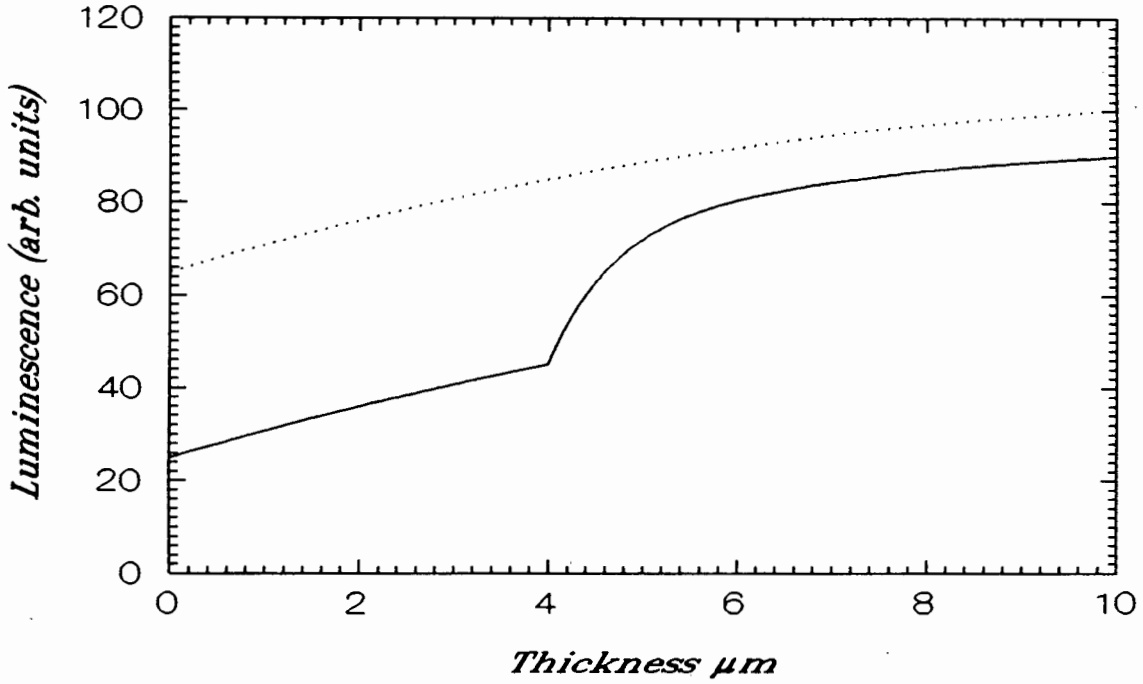

Figure 22 Predicted total luminescent response of the glass based films before and after annealing.

The above analysis will work well for a linear polymer (NE102A) whose individual polymer molecules undergoes complete dissociation in solution, but will need modification when dealing with cross linked polymers such as NE118. Network polymers do not undergo complete dissociation in solution but remain a single network structure (§3.3). The network polymer still behaves like a solution with the individual polymer molecules that make up the chain still able to move. In the presence of the surface orienting force, these individual polymer molecules become lined up along the general direction of the force and, in a similar way, if the thickness of the film is less than the range of the surface orienting force then the whole film will display an ordered structure. Surface layers will thus also occur in NE118 because the physics that govern the formation of these layers in NE102A are exactly the same in NE118. The range of the surface orienting force α in NE118 may be different to that in NE102A because the range of these forces depends on the type of liquid lying above the surface. For films of NE118 thicker than α the film will consist of two regions, as was the case for the NE102A films. The NE118 films cannot, however, solidify with two separate regions. This is because the films consist of a single network. As has been seen in the case of NE102A, the molecules that get packed into a surface region have a higher potential energy than the bulk regions. If the NE118 were to pack into a surface region and a bulk region in the same film, then one part of the network would be at a higher potential energy than another part, and this cannot happen, because the network will tend to even out any differences in potential energy so that the potential energy is the same throughout the network. Thus at any time the network polymer will pack itself into one kind of structure only. In the case of the thin films this means that network polymer NE118 will either have a surface structure across its entire thickness, or a bulk structure across its entire thickness, and for films thicker than α this implies that the film

should behave as though it were all bulk. It is expected that the luminescent step in the NE118 films will be much sharper than in NE102A because the film effectively flips between two structures at a critical thickness T_c. The equations that have been derived to predict the behaviour of the total luminescence as a function of total film thickness will still describe the luminescence of the NE118, but now $T_o=0$. This implies that, for NE118 in the two part function for the luminescence, the same

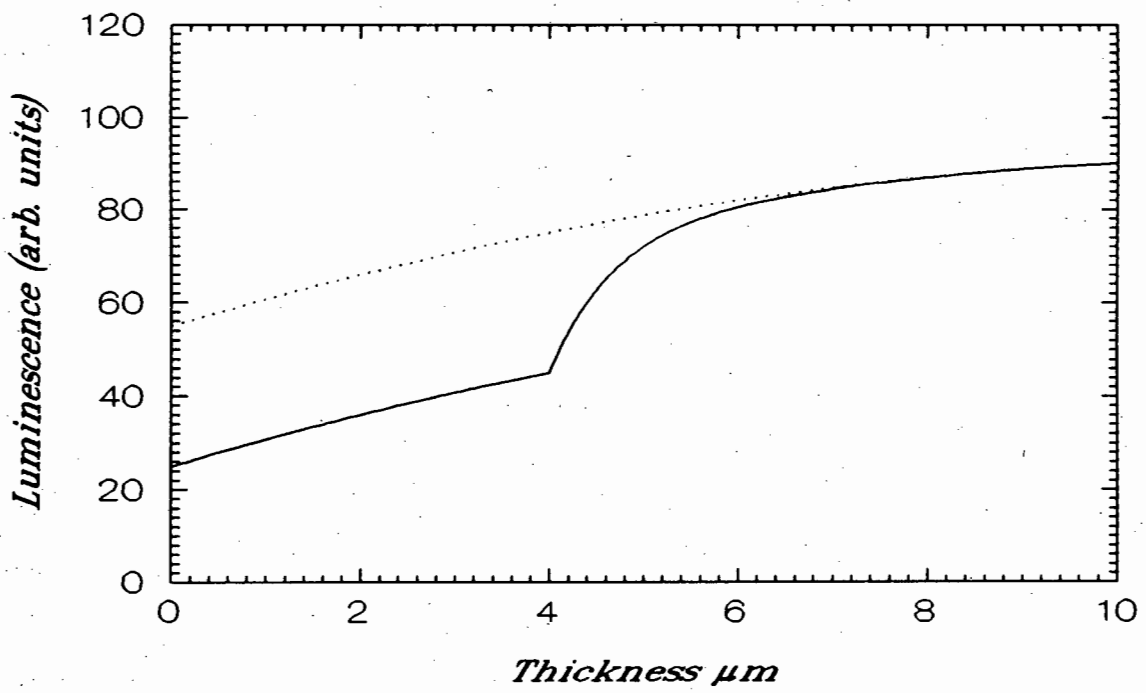

Figure 23 Predicted total luminescent behaviour of the NE118 glass based films before (solid line) and after annealing (broken line).

§5.5 EXPERIMENTAL RESULTS AND PREDICTIONS OF THE MODEL

Figure 24 shows comparison of the non-annealed and annealed GBF of NE102A. The observed behaviour can be accounted for by the above hypothesis.

The annealing has removed the surface layer, and the L versus T response curve shows the same behaviour seen in the WBF and PF. When comparing this to the non-annealed GBF, it can be seen that the region below 5 μm corresponds to the film being composed entirely of surface region, and that above 6 μm, the surface layer was thinner than below 5 μm. Between 5 and 6 μm there is a transition region over which the surface region changes in thickness. We have fitted the semi-empirical equation derived above to the data on the L versus T response of the NE102A and the NE118 non-annealed GBF. The parameters A and B in equation 29 for both the NE102A and the NE118 films are determined by the condition that, on heating the films, the L versus T response function should be exactly the same as that for the annealed-GBF. The parameters A and B are thus fixed at their corresponding values obtained for the annealed-GBF.

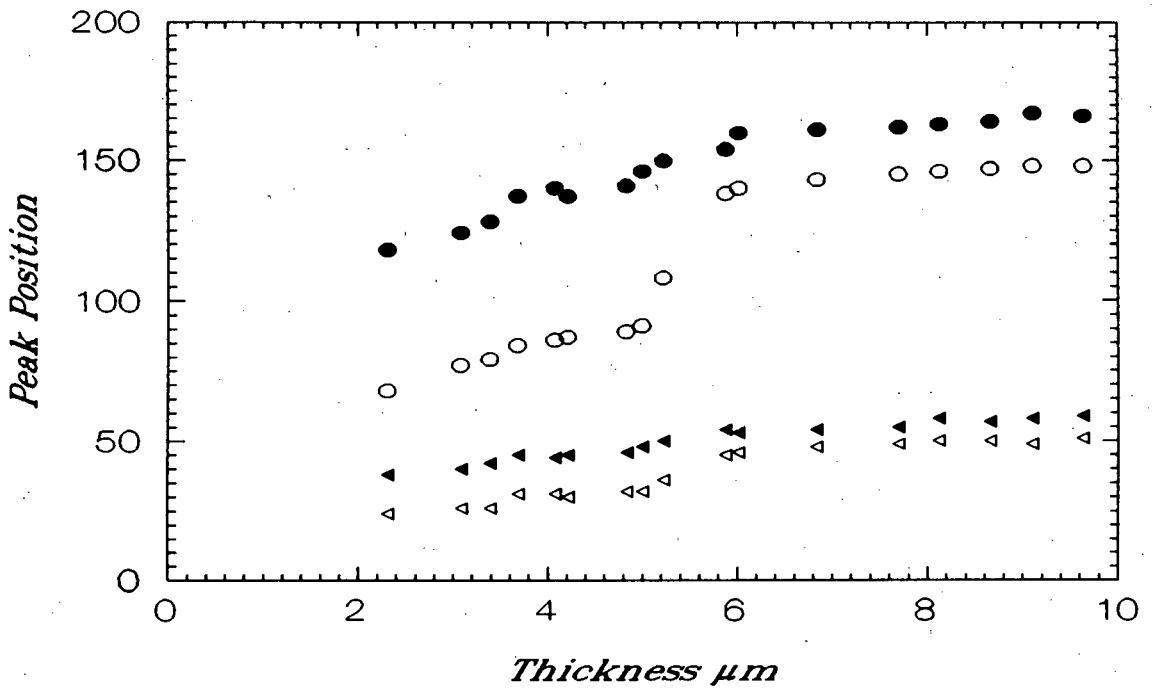

Figure 24 Comparison of L versus T response of NE102A non-annealed (open points) and annealed (filled points) GBF.

Figure 25 shows the L versus T response of the NE102A non-annealed GBF. The critical distance T_c was fixed at 5.0 μm.

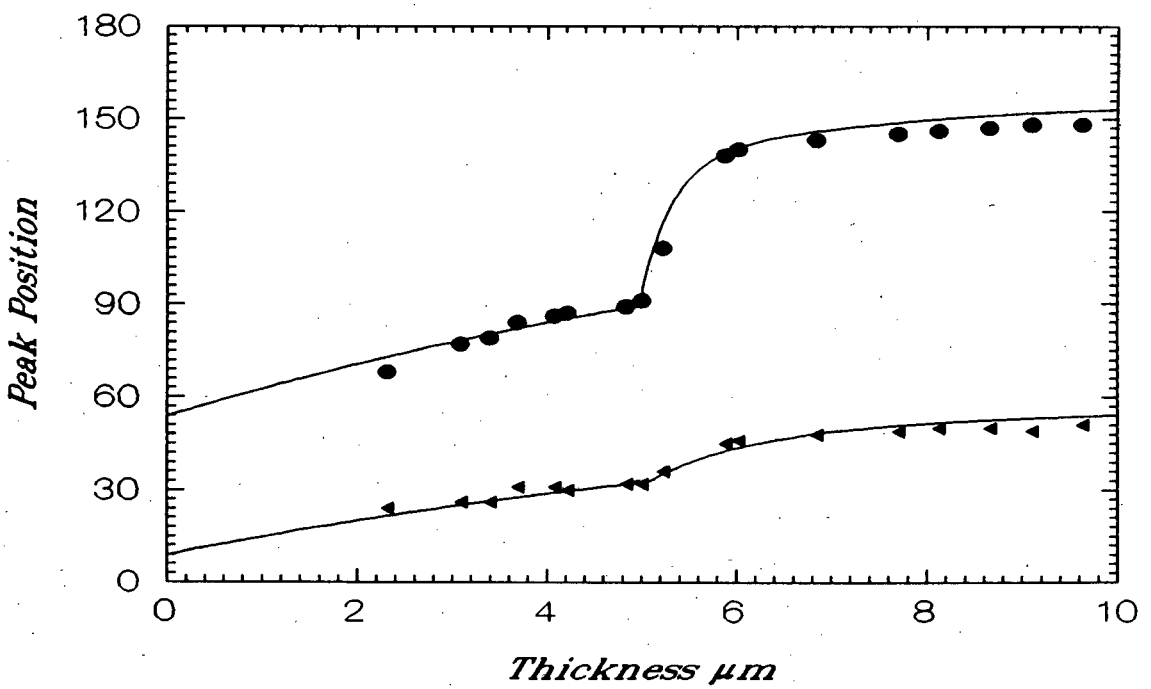

Figure 25 Comparison of the L versus T response of non-annealed GBF of NE102A with the predictions of equation 29

The semi-empirical function provides a good fit to the data. The parameters of the fitted functions for both the mean light and mean heavy fragment are

A_{light}	= -0.29	A_{heavy}	= -0.28
B_{light}	= 8.09	B_{heavy}	= 6.12
C_{light}	= 102.4	C_{heavy}	= 20.90
$C_{b(light)}$	= 53.71	$C_{b(heavy)}$	= 8.88
η_{light}	= 44.08	η_{heavy}	= 13.00
κ_{light}	= -2.92	κ_{heavy}	= -1.20

Figure 26 shows the comparison of the non-annealed and annealed GBF of NE118.

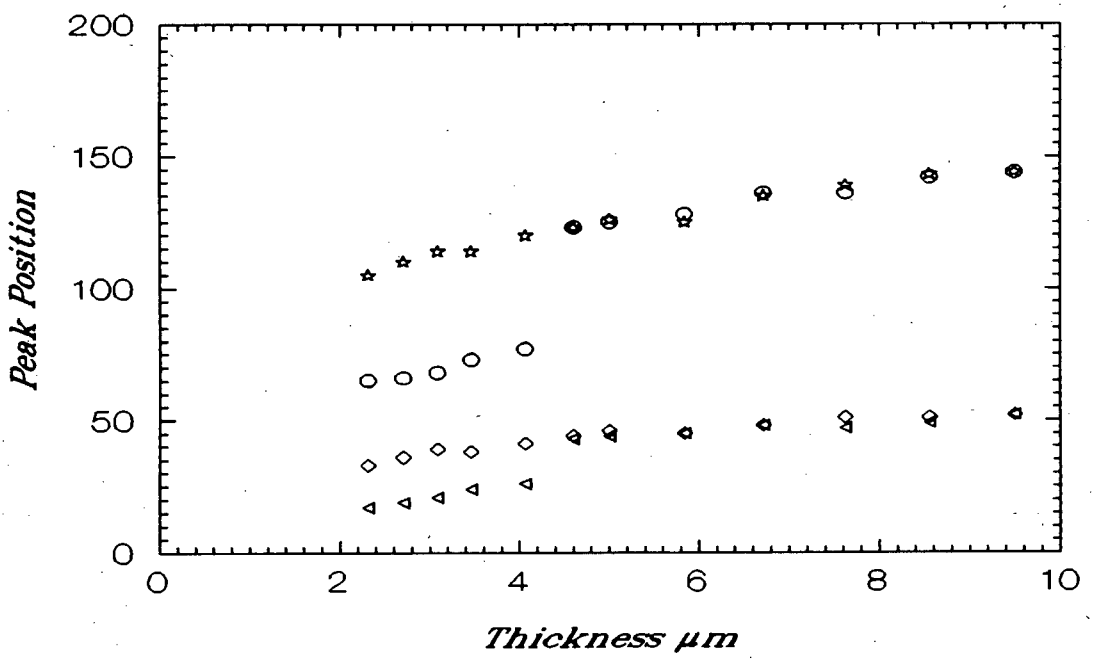

Figure 26 Comparison of L versus T response of non-annealed GBF (circles,triangles) and annealed GBF (stars,diamonds) on NE118.

The comparison indicates that the observations are in agreement with the hypothesis. Below 4.2 μm, the film is composed entirely of surface region. Above 4.5 μm the annealing indicates that there was no surface layer present in the non-annealed GBF above this thickness. This is consistent with the predictions for the behaviour of network polymers. Figure 27 shows the L versus T response of the NE118 non-annealed GBF. The semi-empirical function of equation 22 has been superimposed over it.The critical distance T_c was fixed at 4.20 μm.

The semi-empirical function once again provides a good fit to the data. The parameters of the fitted functions for both the mean light and mean heavy fragment are

A_{light}	= -0.29	A_{heavy}	= -0.28
B_{light}	= 8.09	B_{heavy}	= 6.12
C_{light}	= 92.65	C_{heavy}	= 18.78
$C_{b(light)}$	= 47.48	$C_{b(heavy)}$	= 4.83
η_{light}	= 67.22	η_{heavy}	= 15.50
κ_{light}	= -7.40	κ_{heavy}	= -5.37

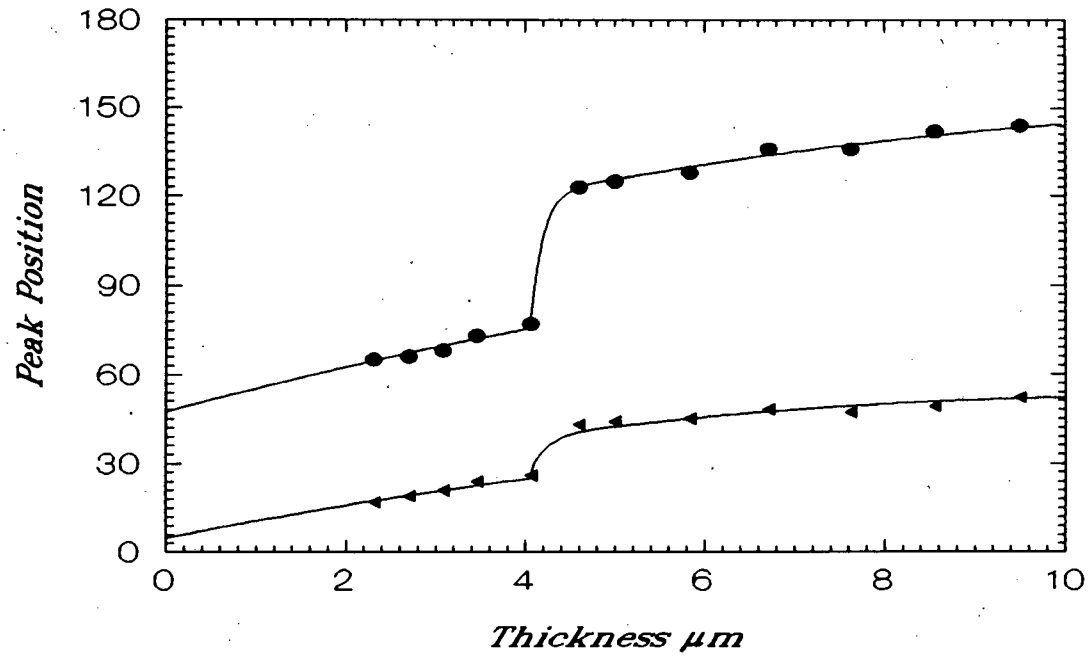

Figure 27 Comparison of the L versus T response of non-annealed GBF of NE118 with the predictions of equation 27

§6 CONCLUSION

We have concluded an extensive investigation into the luminescent behaviour of thin films of NE102A and NE118 plastic scintillators. We have investigated the luminescent response (L) as a function of film thickness (T). During this investigation we have examined 4 different methods of preparing these films, and have compared the luminescent response of each. The 4 methods of preparation were; films prepared on water (WBF), films prepared by pressing them in a specially designed film press (PF), films prepared on a glass surface (non-annealed GBF), and films prepared on a glass surface and then annealed in the film press (annealed GBF). In §2.5 we introduced the Birks relation, the standard formula for predicting L versus T behaviour in materials. We have quoted previous works indicating that the L versus T response of both the NE102A and NE118 thin films should follow this form. We have used the Birks relation and suitably modified it so that the expected luminescent behaviour, in the limit of small dE/dx, was expressed in terms of our experimental variables. The maximum thickness of the films were chosen to minimise saturation effects. The results of our investigations can be placed in two groups. For both the NE102A and NE118 films, the WBF, PF and annealed GBF shows a smooth L versus T response. These responses are in agreement with the predictions of the Birks formula. Both the NE102A and NE118 non-annealed GBF shows a non-linear, step-like L versus T response. This response is not consistent with the predictions of the Birks formula. These results confirms the findings of Brooks[9] and McLeod[10] for NE102A thin films, and to our knowledge, are the first recorded observations of a non-linear, step-like response in thin films of NE118.

The non-linear luminescent response of the non-annealed GBF cannot be accounted for by the Birks formula. The observations can also not be explained in terms of surface quenching effects. By having carefully selected the maximum film thickness, saturation effects in the films could be excluded as an explanation for the observations. Careful consideration of the results has led us to conclude that the origin of the non-linear behaviour in the non-annealed GBF lies in the film being produced on a glass surface. In §5.3 we quoted extensively previous studies indicating that the presence of a solid influences the structure of the liquid lying above it, and that such changes can be transferred to a solid that forms from the liquid. When transferred to a solid, these induced changes produce a distinctive surface region. These surface regions may have properties very different to that of the bulk material. In §3.4 we quoted previous studies indicating that under certain conditions, polymers may develop distinctive surface regions. These have been the basis of the model we have proposed to explain the observed results. Our model proposes that the presence of the glass surface when the non-annealed GBF solution lies on it influences the structure of the liquid lying above it, and this leads to the formation of a surface region in the solidified film. This surface region will have properties different to that of the bulk, in particular, it may have a lower scintillation efficiency. We have produced an expression (§5.4) describing the variation of this surface region with overall film thickness. We have reworked the Birks formula for predicted luminescence to take into account the existence of this proposed surface region, and its variation with overall film thickness, and we have produced a revised formula for the predicted L versus T response. This revised formula is the Birks formula with an added term to account for the possible presence of surface regions. In §5.5 we

have fitted the model to our experimental results, and have found agreement between the predictions and the results.

In light of our findings, it is proposed that the assumption of homogeneity in the structure of thin films is incorrect, and that the behaviour of thin film plastic scintillators is dependent on the method in which they were prepared.

§7 COMPLETE DATA SETS

The following pages contains the eight complete data sets that comprise the work of this study. A total of 94 individual spectra were recorded and used in the analysis. The average collection time of each of these spectra was 14.8 hours, and the average number of counts in each spectra was more than 49 000 counts. The total number of events analysed in this study exceeded 4.5 million, and the total collection time was 1391 hours. The methods for determining the errors on the film thicknesses and the individual peak positions can be found in the appropriate sections (§4). The errors in the data sets are all 1 standard deviation. The following symbols have been used in describing the data sets on the following pages.

$T(\mu m)$	Film thickness (μm).
$\Delta T(\mu m)$	Error on film thickness (μm).
P_{light}	Peak position of the light fragment (arb. units).
ΔP_{light}	Error on P_{light} (arb. units).
P_{heavy}	Peak position of the heavy fragment (arb. units).
ΔP_{heavy}	Error on P_{heavy} (arb. units).

NE102a non-Annealed Glass Based Films.

T(μm)	ΔT(μm)	P_{light}	ΔP_{light}	P_{heavy}	ΔP_{heavy}
2.31	0.15	68	0.10	24	0.04
3.08	0.15	77	0.12	26	0.05
3.39	0.15	79	0.12	26	0.05
3.68	0.15	84	0.11	31	0.05
4.07	0.15	86	0.12	31	0.05
4.21	0.15	87	0.12	30	0.05
4.82	0.15	89	0.13	32	0.06
5.00	0.15	91	0.12	32	0.05
5.22	0.15	108	0.13	36	0.06
5.87	0.15	138	0.14	45	0.06
6.01	0.15	140	0.14	46	0.06
6.84	0.15	143	0.17	48	0.08
7.69	0.15	145	0.15	49	0.06
8.12	0.15	146	0.15	50	0.06
8.65	0.15	147	0.16	50	0.06
9.09	0.15	148	0.15	49	0.06
9.62	0.15	148	0.16	51	0.07

NE102a Annealed Glass Based Films.

T(μm)	ΔT(μm)	P_{light}	ΔP_{light}	P_{heavy}	ΔP_{heavy}
2.31	0.15	118	0.11	39	0.04
3.08	0.15	124	0.12	41	0.05
3.39	0.15	128	0.11	43	0.05
3.68	0.15	137	0.12	45	0.04
4.07	0.15	140	0.13	44	0.05
4.21	0.15	137	0.12	45	0.06
4.82	0.15	141	0.12	46	0.05
5.00	0.15	146	0.13	48	0.06
5.22	0.15	150	0.13	50	0.06
5.87	0.15	154	0.14	54	0.07
6.01	0.15	160	0.15	53	0.07
6.84	0.15	161	0.14	54	0.08
7.69	0.15	162	0.16	55	0.07
8.12	0.15	163	0.15	57	0.08
8.65	0.15	164	0.16	56	0.08
9.09	0.15	167	0.15	57	0.09
9.62	0.15	166	0.15	59	0.09

NE102a Water Based Films

T(μm)	ΔT(μm)	P_{light}	ΔP_{light}	P_{heavy}	ΔP_{heavy}
2.75	0.15	57	0.13	23	0.06
3.43	0.15	63	0.16	24	0.08
3.87	0.15	68	0.15	26	0.07
4.10	0.15	69	0.16	27	0.07
5.21	0.15	76	0.17	32	0.08
6.48	0.15	84	0.17	36	0.08
6.91	0.15	85	0.18	36	0.08
8.65	0.15	90	0.19	39	0.09
10.36	0.15	93	0.18	41	0.08

NE102a Pressed Films

T(μm)	ΔT(μm)	P_{light}	ΔP_{light}	P_{heavy}	ΔP_{heavy}
3.49	0.22	58	0.12	23	0.05
4.29	0.20	63	0.14	26	0.06
4.51	0.20	65	0.13	28	0.06
5.03	0.20	68	0.12	30	0.05
5.48	0.20	70	0.13	31	0.06
6.45	0.21	73	0.15	34	0.07
7.37	0.23	74	0.13	36	0.06
8.75	0.24	81	0.14	41	0.07
10.01	0.26	86	0.15	43	0.07

NE118 non-Annealed Glass Based Films

T(μm)	ΔT(μm)	P_{light}	ΔP_{light}	P_{heavy}	ΔP_{heavy}
2.31	0.15	65	0.12	17	0.06
2.70	0.15	66	0.12	19	0.06
3.08	0.15	68	0.13	21	0.06
3.45	0.15	73	0.12	24	0.06
4.05	0.15	77	0.13	26	0.07
4.59	0.15	123	0.15	43	0.07
4.99	0.15	125	0.16	44	0.08
5.83	0.15	128	0.16	45	0.07
6.71	0.15	136	0.15	48	0.07
7.62	0.15	136	0.17	47	0.09
8.55	0.15	142	0.16	49	0.08
9.49	0.15	144	0.16	52	0.08

NE118 Annealed Glass Based Films

T(μm)	ΔT(μm)	P_{light}	ΔP_{light}	P_{heavy}	ΔP_{heavy}
2.31	0.15	105	0.12	33	0.06
2.70	0.15	110	0.13	36	0.07
3.08	0.15	114	0.13	39	0.07
3.45	0.15	114	0.12	38	0.06
4.05	0.15	120	0.13	41	0.07
4.59	0.15	123	0.15	44	0.07
4.99	0.15	126	0.17	46	0.08
5.83	0.15	125	0.16	45	0.07
6.71	0.15	135	0.16	48	0.08
7.62	0.15	139	0.17	51	0.09
8.55	0.15	143	0.17	51	0.09
9.49	0.15	144	0.16	52	0.08

NE118 Water Based Films

T(μm)	ΔT(μm)	P_{light}	ΔP_{light}	P_{heavy}	ΔP_{heavy}
2.90	0.15	57	0.11	19	0.05
3.84	0.15	64	0.12	22	0.06
5.07	0.15	73	0.13	25	0.06
5.67	0.15	75	0.13	26	0.06
6.72	0.15	80	0.12	30	0.06
8.25	0.15	88	0.14	36	0.07
8.75	0.15	91	0.13	38	0.06
9.45	0.15	92	0.15	40	0.07
10.64	0.15	96	0.18	42	0.08

NE118 Pressed Films

T(μm)	ΔT(μm)	P_{light}	ΔP_{light}	P_{heavy}	ΔP_{heavy}
3.54	0.22	58	0.14	19	0.06
4.43	0.20	64	0.16	22	0.07
5.50	0.20	69	0.16	24	0.07
6.41	0.20	71	0.15	27	0.06
6.94	0.21	74	0.16	27	0.07
8.17	0.22	84	0.17	34	0.08
9.09	0.24	91	0.18	36	0.09
10.29	0.26	97	0.20	42	0.09

§8 REFERENCES

1 Muga M.L, Burnsed D.J, Steeger W.E, Taylor H.E
Nucl. Instr. Meth. 83(1970)135

2 Muga M.L, Burnsed D.J, Steeger W.E
Nucl. Instr. Meth. 104(1972)605

3 Muga M.L, Griffith G.L, Schmitt H.W, Taylor H.E
Nucl. Instr. Meth. 111(1973)581

4 Muga M.L, Clem A, Griffith G, Plendl H.S, Eaker R, Holub R
Nucl. Instr. Meth. 119(1974)255

5 Batsch T, Moszynski M
Nucl.Instr. Meth. 123(1975)341

6 Birks J.B
Theory and Practice of Scintillation Counting
Pergammon Press Ltd., London, 1964

7 Batra R.K, Shotter A.C
Nucl. Instr. Meth. 124(1975)101

8 Ajitanand N.N, Iyengar K.N
Nucl. Instr. Meth. 133(1976)71

9 Brooks F.D, Cilliers W.A.C, Allie M.S
Nucl. Instr. Meth. A240(1985)338

10 McLeod J.M
University of Cape Town (unpublished)

11 Pringsheim P
Flouresence and Phosphoresence
Interscience, New York, 1949

12 King T.A, Voltz R
Proc. Roy. Soc A289(1966)424

13 Brooks F.D
Nucl. Instr. Meth. 162(1979)477

14 Brooks F.D
Prog. Nucl. Phys. 5(1956)252

15 Koski W.S
Phys. Rev. 84(1951)852

16 Ageno M, Cortelessa G
Nuovo Cimento 9(1952)196

17 Ageno M, Querzoli R
Nuovo Cimento 9(1952)282

18 Birks J.B, Kuchela K.N
Disc. Faraday. Soc. 7(1959)57

19 Forster T
Disc. Faraday. Soc. 7(1959)7

20 Swank R.K, Buck W.L
Phys. Rev. 91(1953)927

21 Basile L.J
Trans. Faraday. Soc. 60(1964)1702

22 Black F.A
Phil. Mag. 44(1953)263
23 Meyer A, Murray R.B
Phys. Rev.
24 Jentschke W.K, Eby F.S, Taylor C.J, Remley M.E, Kruger P.G
Phys. Rev. 83(1951)170
25 Birks J.B
Phys. Rev. 86(1952)569
26 Birks J.B
Phys. Rev. 90(1953)1131
27 Wright G.T
Phys. Rev. 100(1955)588
28 Wright G.T
Proc. Phys. Soc. B68(1955)701
29 Taylor C.J, Jentschke W.K, Remley M.E, Eby F.S, Kruger P.S
Phys. Rev. 84(1951)1034
30 Schram E
Organic Scintillation Detectors
Elsevier, New York, 1963
31 Birks J.B
Proc. Phys. Soc. A64(1951)874
32 Chou C.N
Phys. Rev. 87(1952)904
33 Furst M, Kallman H
Phys. Rev. 85(1952)816
34 Wright G.T
Phys. Rev. 91(1953)1282
35 Voltz R, Lopez da Silva J, Laustrait G, Coche A
J. Chem. Phys. 45(1966)3306
36 Newman E, Smith A.M, Steigert F.E
Phys. Rev. 122(1961)1520
37 Muga H, Griffith G
Phys. Rev. B9(1974)3639
38 Segre E
Experimental Nuclear Physics, Vol 1
John Wiley, New York, 1953
39 Bell G.I
Phys. Rev. 90(1953)548
40 Bohr N
Phys. Rev. 59(1941)270
41 Fulmar C.B, Cohen B.L
Phys. Rev. 109(1958)94
42 Fulmar C.B
Phys. Rev. 108(1957)1113
43 Whetstone S.L
Phys. Rev. 131(1963)1232

44 Fink J
Can. J. Chem. 39(1961)646
45 Northcliff L.C, Schilling R.F
Nucl. Data Tables 7(1970)233
46 Roberts J.D, Stewart R, Caserio M.C
Organic Chemistry
Addison Wesley, New York, 1972
47 Young R.T
Introduction to Polymers
Chapman and Hall, London, 1981
48 Flory P.J
J. Chem. Phys. 13(1945)453
49 Kuhn W, Kuhn H
Helv. Chim. Acta. 26(1943)1394
50 Flory P.J
Principles of Polymer Chemistry
Cornell University Press, New York, 1953
51 Keller A, Machin M.J
Macr. Phys. 1(1966)27
52 Palin G.R
Plastics for Engineers
Pergammon, New York, 1967
53 Hall C
Polymer Materials
MacMillan, London, 1989
54 Eby R.K
J. Appl. Phys. 35(1964)2720
55 Kwei T.H, Schornhorn H
J. Appl. Phys. 38(1967)2512
56 Fritsch H.L, Gaines G.L, Schornhorn H
Surfaces, Vol 6B, 343
Plenum Press, New York, 1976
57 Largiss C
Nucleonics 14(1956)66
58 Flannery B.P, Press H.P, Teukolsky S.A, Vettering W.T
Numerical Recipes in C
Cambridge University Press, Cambridge, 1988
59 Flannery B.P, Press H.P, Teuklosky S.A, Vettering W.T
Numerical Recipes Example Book
Cambridge University Press, Cambridge, 1988
60 Derjaguin B
Nature 138(1936)330
61 Taylor A.M, King A
Nature 132(1933)64
62 Hardy W.B
Proc. Roy. Soc. A86(1912)631

63 McHaffie I.R, Lenher S
J. Chem. Soc. 127(1925)1559
64 Lenher S
J. Chem. Soc. 129(1927)272
65 Joris G.G, Taylor H.S
J. Chem. Phys. 16(1948)45
66 Henniker J.C
Rev. Mod. Phys. 21(1949)322
67 Brummage K.G
Proc. Roy. Soc. A191(1947)243
68 McBain J.W
N.A.C.A, Washington (Colloid Science pp70, Boston, 1950)
69 Watson H.E, Menon A.S
Proc. Roy. Soc. A123(1929)185
70 Wilson R.E, Barnard D.P
Ind. Eng. Chem. 14(1922)683
71 Bowden F
Physik. Zeits. 4(1933)185
72 Duff A.W
Phil. Mag. 9(1905)685
73 Shereshefsky J.L
J. Am. Chem. Soc. 50(1928)2966
74 Rothen A
J. Biol. Chem. 168(1947)75
75 Rothen A
J. Biol. Chem. 163(1946)345
76 Rothen A
J. Biol. Chem.
77 Bradley R.S
Z. Krist. 96(1937)499
78 Finch G.I
Nature 140(1937)800
79 McBain J.W
Colloid Science
B.C Heath, Boston, 1950
80 Adamson A.W
Physical Chemistry of Surfaces
Interscience, New York, 1967

ACKNOWLEDGEMENT

A special thank you to my supervisor, Dr Willem Cilliers, for his guidance, suggestions and assistance during the course of my masters, but most of all, a very big thank you to WAC for putting up with me for the past three years.